

## AN ABSTRACT OF THE THESIS OF

Marcel Merk for the degree of Master of Science in Electrical & Computer Engineering  
presented on October 4, 2000. Title: Active Power Filter for the Cancellation of  
Harmonic Line Current Distortion.

Redacted for Privacy

Abstract approved: \_\_\_\_\_

Annette R. von Jouanne

With the increased attention on high efficiency and energy savings, power electronic energy conversion equipment is increasingly incorporated in all levels of the power system. The drawback of such equipment is the generation of nonsinusoidal currents in the power distribution network due to the nonlinear operation. Harmonic currents may distort the line voltages and lead to several unwanted effects including equipment overheating, system failure, interference with communication systems, etc.

In response to these concerns, this research presents an active filter for the cancellation of harmonic line current distortion. The active filter used in this research is connected in parallel with the nonlinear load and is designed for a three-phase three-wire industrial power system. The filter consists of a voltage source inverter connected through a coupling inductor to the terminals of the *ac*-source. The inverter is controlled via a space vector-pulse width modulation (*SVPWM*) algorithm that is generated using a digital signal processor (*DSP*). In order to reduce the distortion resulting from the switching nature of the active filter inverter, a switching ripple filter is connected in parallel.

The control algorithm of the active filter is based on the rotating reference frame theory. For each harmonic which is to be cancelled, a corresponding synchronous reference frame is generated to extract the harmonic phase and magnitude. With this information, each harmonic current component can be separately controlled and the proposed algorithm can therefore compensate for hardware effects such as measuring de-

lays and component transfer functions. For the extraction of the harmonic components, a finite impulse response filter is used in order to quickly react to changing load currents. An adapting algorithm is implemented to compensate for slowly varying system parameters.

Simulations under varying load and transient conditions are performed. The results show nearly perfect cancellation performance for the proposed active filter control algorithm.

©Copyright by Marcel Merk

October 4, 2000

All rights reserved

Active Power Filter  
for the Cancellation of  
Harmonic Line Current Distortion

by

Marcel Merk

A THESIS

submitted to

Oregon State University

in partial fulfillment of  
the requirements for the  
degree of

Master of Science

Presented October 4, 2000  
Commencement June 2001

Master of Science thesis of Marcel Merk presented on October 4, 2000

APPROVED:

Redacted for Privacy

Major Professor, representing Electrical & Computer Engineering

Redacted for Privacy

Chair of Department of Electrical & Computer Engineering

Redacted for Privacy

Dean of Graduate School

I understand that my thesis will become part of the permanent collection of Oregon State University libraries. My signature below authorizes release of my thesis to any reader upon request.

Redacted for Privacy

Marcel Merk, Author

## ACKNOWLEDGMENT

I would like to express my gratitude to Hans and Adele Neukomm for their remarkable program that made it possible for me to study in the United States. I wish both the Neukomm's and the program continued success in the future.

I would like to thank Dr. Annette von Jouanne for her assistance during my study at Oregon State University. I was impressed by her enthusiasm and dedication to the field of power electronics. I would also like to thank the other members of my committee, Dr. Molly Shor, Dr. Alan Wallace, and Dr. Jim Coakley. I would like to thank Evelyn Matheson and Abdurrahman Unsal for their patience with my personality and for their comments on multiple drafts of my thesis.

Most of all, I would like to thank my family for their continued guidance and support, and my friends, especially Tobias Bathon, for their laughter and solace when dealing with difficult cultural adjustments.

## TABLE OF CONTENTS

	<u>Page</u>
1. INTRODUCTION .....	1
1.1. Power Quality .....	1
1.1.1. What is Power Quality?.....	1
1.1.2. Harmonic Current Distortion.....	3
1.2. Harmonic Filtering.....	5
1.3. Research Project.....	7
1.3.1. Research Objectives.....	7
1.3.2. Research Steps.....	8
1.3.3. Thesis Organization.....	9
2. REFERENCE FRAME THEORY .....	11
2.1. Introduction and Motivation .....	11
2.2. Transformations.....	12
2.2.1. Stationary Reference Frame .....	12
2.2.2. Rotating Reference Frame.....	14
2.2.3. $pq$ -Transformation .....	15
2.2.4. Transformation of Harmonic Current .....	16
2.3. Space Vector Pulse Width Modulation .....	17
3. ELECTRICAL SYSTEM .....	20
3.1. Introduction .....	20
3.2. Power Circuit.....	21
3.2.1. Source and Load .....	22
3.2.2. Active Filter Circuit .....	25
3.2.3. Switching Ripple Filter .....	27

## TABLE OF CONTENTS (Continued)

	<u>Page</u>
3.3. DSP Interface.....	28
3.3.1. Interface Circuits .....	29
3.3.2. Transfer Characteristic.....	31
4. CONTROL SCHEME .....	33
4.1. Compensation with Ideal Hardware .....	33
4.1.1. Compensation in Delayless System .....	33
4.1.2. Effects due to Delayed Current Injection .....	35
4.2. Block Diagram .....	36
4.3. Control Strategy .....	38
4.3.1. Overview .....	38
4.3.2. Fundamental Control .....	39
4.3.3. Harmonic Controller .....	43
4.4. Reference Frame Generator .....	45
4.5. Simulation .....	47
4.5.1. General .....	47
4.5.2. Startup of Power Circuit .....	47
4.5.3. Steady State Compensation .....	50
4.5.4. Transient Behavior.....	52
4.5.5. Switching Ripple Filter .....	54
5. SUMMARY OF RESULTS .....	56
5.1. Discussion .....	56
5.2. Conclusions.....	57
5.3. Future Recommendation .....	58



## TABLE OF CONTENTS (Continued)

	<u>Page</u>
BIBLIOGRAPHY .....	59
APPENDICES .....	62
A GRAPH CREATION AND SPECTRA CALCULATION .....	64
B NOMENCLATURE .....	65
C COMPLETE SIMULATION CIRCUIT DIAGRAM .....	68
D SIMULATION FILES .....	69
E LIST OF MATERIALS FOR HARDWARE EVALUATION .....	77

## LIST OF FIGURES

<u>Figure</u>	<u>Page</u>
1.1 Power system with various distributed loads and point of common coupling ( <i>PCC</i> ). . . . .	4
1.2 Basic principle of a shunt active filter. . . . .	6
1.3 Basic principle of a series active filter. . . . .	7
2.1 Inverter bridge used for active filter. . . . .	17
2.2 The eight voltage vectors characterizing the inverter operation. . . . .	18
2.3 Symmetric space vector <i>PWM</i> waveform. . . . .	19
3.1 Block diagram of the hardware. . . . .	20
3.2 Load and source configuration. . . . .	21
3.3 Source voltage $v_{sa}$ and load current $i_{ra}$ . . . . .	23
3.4 Spectrum of load current $i_{ra}$ . . . . .	23
3.5 Total harmonic distortion $THD_{i_r}$ under different load conditions. . . . .	24
3.6 Active filter circuit with switching ripple filter. . . . .	25
3.7 Frequency response of switching filter ripple $Z_v(j\omega)$ . . . . .	28
3.8 Block diagram of input interface circuit. . . . .	29
3.9 Frequency response of anti aliasing filter $H_A(j\omega)$ . . . . .	30
3.10 Block diagram of output interface circuit. . . . .	30
3.11 Block diagram control system. . . . .	31
3.12 Timing diagram. . . . .	32
4.1 Ideal compensation principle. . . . .	33
4.2 Separated fundamental and harmonic current. . . . .	34
4.3 Effect on delayed compensation current injection (left: $t_d = T_T$ , right: $t_d = 2T_T$ ). . . . .	36
4.4 Block diagram of active filter. . . . .	37
4.5 Control strategy overview. . . . .	38

## LIST OF FIGURES (Continued)

<u>Figure</u>	<u>Page</u>
4.6 Control circuit for fundamental current.....	40
4.7 Bode-diagram of linear phase <i>FIR</i> -filter for fundamental and harmonic extraction. ....	41
4.8 Bode-diagram of <i>IIR</i> -filter for adaption algorithm. ....	42
4.9 Control circuit for one harmonic current component. ....	43
4.10 Phase-locked-loop with phase discriminator ( <i>PD</i> ) and voltage controlled oscillator ( <i>VCO</i> ).....	46
4.11 System currents at startup. ....	48
4.12 Adaption of fundamental correction factor.....	48
4.13 Adaption of harmonic correction factors. ....	49
4.14 Source and compensation currents.....	51
4.15 Active filter and switching ripple filter currents. ....	52
4.16 Currents during a load transient. ....	53
4.17 Current spectra after load transient. ....	54
4.18 Unfiltered compensation and source current. ....	55
4.19 Wideband spectra of active filter, compensation, and source current. ...	55

## LIST OF TABLES

<u>Table</u>	<u>Page</u>
2.1 Inverter switching combination and corresponding output voltage. ....	18
3.1 Simulation parameters. ....	22
3.2 Simulation results. ....	24
3.3 Simulation parameters for active filter. ....	26
4.1 Phase shift due to system delays of $t_d = T_T$ and $t_d = 2T_T$ . ....	35
4.2 Initial and final values of adaption parameters. ....	49
4.3 Resulting system currents. ....	51
4.4 Resulting system currents after load transient. ....	54

## LIST OF APPENDIX FIGURES

<u>Figure</u>	<u>Page</u>
C.1 Complete simulation circuit diagram. ....	68
D.1 <i>SIMULINK</i> model: Top level with <i>PLECS</i> circuit interface and data recording. ....	69
D.2 <i>SIMULINK</i> model: Control algorithm. ....	69
D.3 <i>SIMULINK</i> model: All harmonic current controllers.....	70
D.4 <i>SIMULINK</i> model: Harmonic current controller for 5th harmonic. ....	70
D.5 <i>SIMULINK</i> model: Fundamental current controller. ....	70

# ACTIVE POWER FILTER FOR THE CANCELLATION OF HARMONIC LINE CURRENT DISTORTION

## 1. INTRODUCTION

### 1.1. Power Quality

#### 1.1.1. *What is Power Quality?*

Both electric utilities and end users of electrical power are becoming increasingly concerned about the quality of electric power [1]. The power industry addressed the issue of power quality beginning in the late 1980s, and intense research has been done since. In contrast to earlier research, engineers are nowadays more interested in solving power quality problems on a system basis rather than as individual problems. Depending on the point of view, there are many different definitions of the term 'Power Quality.' The term 'power quality problem' is defined in [1] as follows:

"Any power problem manifested in voltage, current, or frequency deviations that results in failure or misoperation of customer equipment."

The main reason that industry is interested in power quality is economic value. The quality of power can have a direct economic impact on customers as well as on utilities. On the customer side, the main concern is to have properly functioning equipment. Unfortunately, modern highly efficient solid state converters are sensitive to power disturbances which may result in malfunction or unintended tripping of protection circuits resulting in down time. These down times are unproductive and therefore cause economic losses. On the other hand, utilities have to guarantee a certain level of power quality to their customers. Utilities are also in strong competition and therefore interested in reducing the cost of generation and distribution of energy. Significant power quality problems

may cause additional losses in distribution lines which require derating of equipment, result in additional down time due to malfunction of protection circuits, etc.

Major power quality problems can be classified as follows [1]:

**Transient:** A transient is that part of a change in a variable that disappears during transition from one steady state operating condition to another. Transients can last a few nano seconds to about 8ms ( $\frac{1}{2}$  cycle) [2].

**Short-duration variation:** Short-duration variations might be caused by fault conditions, startup of large loads, or intermittent loose connection of power wiring. In contrast to transients, these kind of variations are much longer in nature, i.e. up to one minute.

**Long-duration variation:** Long-duration variations encompass root-mean-square (*rms*) deviations at power frequencies for longer than one minute.

**Voltage imbalance:** Voltage imbalance can be defined as the deviation from the average of the three-phase voltages or currents. It also can be defined using symmetrical components. Voltage imbalances are considered a steady-state condition.

**Waveform distortion:** Waveform distortion is defined as a steady-state deviation from an ideal sine wave. There are five primary types of waveform distortions: *dc* offset, harmonics, interharmonics, notching, and noise.

**Voltage fluctuation:** Voltage fluctuations are systematic variations of the voltage envelope. These are intermittent occurrences of a typical spectral content  $< 25Hz$ .

**Power frequency variation:** Power frequency variations are defined as the deviation of the power system fundamental frequency from its specified nominal value (e. g. 50 or 60Hz).

### 1.1.2. *Harmonic Current Distortion*

Harmonic current distortion originates from nonlinear characteristics of devices and loads on the power system. Several common past and current harmonic current sources are given below [3], [4]:

- Transformer magnetizing currents
- Cycloconverters used for low-speed, high-torque machines
- Network nonlinearities from loads such as solid-state converters, arc-welders, etc.
- Electrochemical processes
- Fluorescent lighting, modulated furnaces

Modern solid-state converters are increasingly contributing to harmonic currents due to increasing use of rectifier front-ends. Also, modern high-technology solid-state equipment is very sensitive to pollution from other harmonic sources. Power electronic equipment is at the same time villain and victim from the power quality point of view [5]. Some common effects of harmonic distortion are [3], [4]:

- Capacitor bank failure from dielectric breakdown or reactive power overload.
- Unstable operation of firing circuits based on voltage zero-crossing detection or latching.
- Errors in induction *kWh*-meters.
- Increased losses and heating in induction and synchronous machines as well as transformers.
- Overvoltage and excessive currents in the system resulting in resonance due to harmonic voltages or currents.
- Signal interference and relay malfunction, particularly in solid-state, microprocessor, and telecommunications systems.



The extent of the listed effects on the load depends on the type of harmonic source, its location in relation to the load, and the power network characteristic.

Harmonic distortion can be described completely by its harmonic spectrum with the magnitude and phase angle of each individual harmonic component. A more quantitative measure of harmonic distortion is the so called total harmonic distortion (*THD*) which is defined as:

$$THD_i = \frac{1}{I_1} \sqrt{\sum_{h=2}^{\infty} I_h^2} = \frac{1}{I_1} \sqrt{I^2 - I_1^2} \quad (1.1)$$

where  $I_1$  is the *rms*-value of the fundamental current component (fundamental),  $I_h$  are the *rms*-values of the harmonic components (harmonics),  $I$  is the *rms*-value of the signal and the subscript  $i$  refers to the *THD* of the current. A similar index  $THD_v$  can be expressed by using voltage components in (1.1). The *THD* is often measured in %, i. e.  $THD_{\%} = THD \cdot 100\%$ .

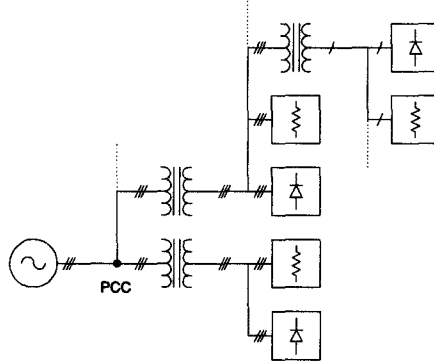


FIGURE 1.1: Power system with various distributed loads and point of common coupling (*PCC*).

To handle the concern of harmonic currents, IEEE Standard 519-1992 [6] provides a guideline for recommended distortion levels of harmonic currents and voltages on power distribution systems at the point of common coupling (*PCC*) (Fig. 1.1). To handle current harmonics in a more consistent fashion, the standard defines another term, the

total demand distortion ( $TDD$ )

$$TDD_i = \frac{1}{I_{demand}} \sqrt{\sum_{h=2}^{\infty} I_h^2} = \frac{1}{I_{demand}} \sqrt{I^2 - I_1^2} \quad (1.2)$$

This term expresses the distortion in relation to the maximum demand load current rather in relation to the fundamental current magnitude.

For completion, two additional power quality measures are defined:

$$DPF = \cos \varphi \quad (1.3)$$

$$PF = \frac{I_1}{I} \cos \varphi = \frac{I_1}{I} \cdot DPF \quad (1.4)$$

where  $DPF$  is the displacement power factor,  $PF$  is the power factor (or true power factor),  $I_1$  is the *rms*-value of the fundamental current component,  $I$  is the *rms*-value of the current, and  $\varphi$  is the phase angle lag of the fundamental current component with respect to the voltage (assuming the voltage is sinusoidal).

## 1.2. Harmonic Filtering

In the past, passive filters consisting of tuned LC filters and/or high-pass filters have been used to improve power factor and suppress harmonics in systems. Unfortunately, passive filters have some major drawbacks [7]:

- The source impedance, which is not accurately known and varies with time, temperature, and system configuration, strongly influences the filtering characteristics of the shunt passive filter.
- The shunt passive filter may act as a sink of harmonic current not only coming from the polluting load but also from the source or other system components. In the worst case, the passive filter may overload with harmonic current and fail.
- At specific frequencies, passive filters may be in parallel resonance with the source or other system elements. This may lead to power system instabilities.

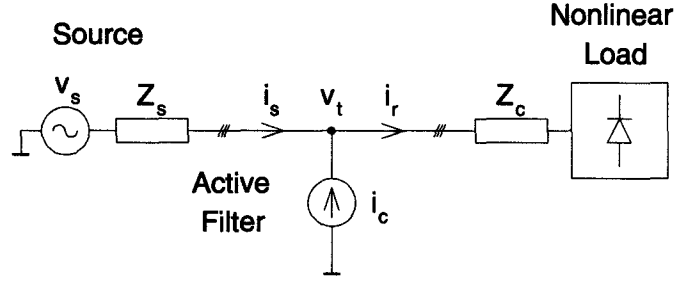


FIGURE 1.2: Basic principle of a shunt active filter.

In order to reduce the negative drawbacks of passive filters, active filters have been introduced. Aside from the basic harmonic current compensation or filtering, active filters may have additional features such as power factor correction, ride-through capability, additional protection, etc.

Active power filters have been studied to compensate for harmonics in industrial power systems since their basic compensation principle was proposed in the 1970's. At that time, there was almost no advancement in active power filters beyond a laboratory testing stage because circuit technology was too poor to practically implement the compensation principles [8]. In the last few years, remarkable progress has been made in the sector of micro processors (*uP*) and digital signal processors (*DSP*). These powerful devices allow the implementation of modern and complex algorithms and the simultaneous measurement and control of several external signals. Some *DSPs* already have up to 16 A/D channels, several D/A channels, and up to 9 pulse width modulation (*PWM*) ports on-chip. These packed devices in combination with new fast power solid-state switches allow for building of small, cost reduced power system equipment. An active filter for a power system application can best be described as [1]:

Any of a number of sophisticated power electronic devices for eliminating harmonic distortion.

Generally, harmonic filters can be divided into three main groups: passive, active, and hybrid filters. In which the latter group is a combination of active and passive filter

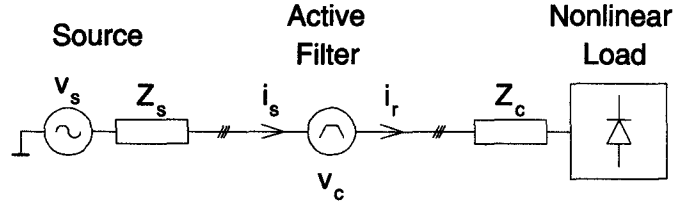


FIGURE 1.3: Basic principle of a series active filter.

components. Each of these groups are subdivided into shunt (or parallel) and series filters. The one-line diagram of a shunt active filter is shown in Fig.1.2, and a series active filter is shown in Fig.1.3 [9] [10].

Shunt active filters are mainly used for eliminating current harmonics, reactive power compensation and balancing unbalanced currents. The filter injects compensating current equal to the load harmonics or reactive current, but with opposite phase to effectively cancel the harmonic or reactive current components flowing towards the source. Series active filters are connected between the source and the load. They mainly act as a harmonic voltage block and can also be used for voltage stabilization.

## 1.3. Research Project

### 1.3.1. Research Objectives

The objectives of this research are to:

- analyze the effects of non-ideal behavior of hardware components such as delays, phase shifts, etc. on the control strategy of an active filter,
- design a controller that can compensate for those non-idealities,
- investigate a possible implementation of the proposed control strategy in a laboratory prototype.

The primary goal of the proposed active filter is to reduce harmonic current distortion in three-phase three-wire systems. The active filter should be able to independently cancel lower order (5<sup>th</sup>, 7<sup>th</sup>, 11<sup>th</sup>, 13<sup>th</sup>) harmonics under varying load conditions. Furthermore, the active filter should react quickly to load changes, i. e. in less than the time of one fundamental period (16.67ms for 60Hz). The control algorithm should not rely on exact hardware parameters, it should be able to adapt to varying parameters.

### 1.3.2. *Research Steps*

During the research, several major project phases have been run through in order to achieve the objectives:

1. Literature research has been done with the main focus on active filter control strategies and implementation. It has been found that published papers mainly focus on the theoretical aspects of active filter control strategies and do not detail the problems occurring in hardware implementation. In this stage, it was decided to focus on a shunt active filter using a voltage source inverter and a coupling inductor. This topology requires minimal number of hardware components, and it does not have to be rated for the full load power. Instead, the filter has only to be rated for the cancellation current and some small amount of power factor correcting current.
2. With simulations in *MATLAB*, *SIMULINK* [11], and *PLECS* [12], the effects of system delays on the effectiveness of the active filter could be analyzed. By including the configuration of the hardware in the simulation, a control strategy that compensates for these delays in the system was found and simulated. Several user defined *SIMULINK* blocks (so called *s-functions*) have been programmed in order to realistically model the hardware behavior, such as space vector *PWM*, phase locked loops (*PLL*), etc.

3. It has been investigated to determine if the control algorithm can be implemented in a laboratory prototype. The investigation has been performed on a *Texas Instruments TMS320F240 DSP*. The active filter power circuit was also built in a prototype manner similar to an existing system used for another active filter implementation [13].

In addition to the major phases mentioned above, assistance has been given to design, assemble and test the hardware labor prototype mentioned above. The hardware implements a complete active filter and is also used to investigate the implementation of the control algorithm in this research.

### 1.3.3. *Thesis Organization*

The contents of the thesis are organized in the following manner. Chapter 1 provides the necessary background information about power quality and the sources and effects of power system harmonics. It also gives a brief outline of filtering topologies and defines the research objectives.

Chapter 2 presents the necessary theoretical background about the reference frame theory as used in this thesis. It also demonstrates the effects on fundamental and harmonic signal components when transformed into different reference frames. The last part of this chapter addresses Space Vector Pulse Width Modulation *SVPWM* which is used for simulation and hardware implementation.

In chapter 3, the electrical system components used for the hardware implementation are explained and analyzed. In the first part, the power system used for simulation and experiment is shown and its harmonic distortion quantized. The designs of the active filter circuit and switching ripple filter are presented. In the second part, the low power control circuit is described including input signal conditioning circuits, anti-aliasing filters, analog-digital converters, space vector control logic, and high power drive circuit. The hardware is explained on a system based level; more detailed information can be found in [13].

Chapter 4 concentrates on the proposed active filter control strategy. The basic idea of compensation with delayless hardware is presented and the effects due to propagation and measuring delays are demonstrated. The designs of the fundamental current controller and harmonic current controller are given. Finally, the reference frame generator using a *PLL* is shown and analyzed in detail.

Chapter 5 is the concluding chapter in which the results and problems are discussed. Suggestions for future work in the area of active harmonic filtering using the proposed system are also included.

The appendices contain nomenclature, complete circuit schematics, flow charts of the programming, code examples, etc.

## 2. REFERENCE FRAME THEORY

### 2.1. Introduction and Motivation

In the late 1920's, R. H. Park introduced a new approach to electric machine analysis [14]. He formulated a change of variables which replaced the variables (voltage, current, etc.) associated with the stator windings of a synchronous machine with variables instead associated with fictitious windings rotating with the rotor, i. e. he referred the stator variables to a frame of reference fixed in the rotor. After Park, many researchers applied the same idea on other machines in order to simplify their control.

With the introduction of solid state power converters, it was found convenient to characterize the inverter in the same framework as used for motors. In order to control active power filters, H. Akagi introduced the so called *pq-theory* or *instantaneous reactive power theory* [15], which in fact is similar to the reference frame theory using a synchronous rotating reference frame. In this project, the approach of using the *pq-theory* has been studied and found that it is an excellent way to cancel harmonics with a low requirement of computational power. Unfortunately, the *pq-theory* has some drawbacks in effectively canceling harmonics if major system delays are present as discussed in Chapter 3. In order to compensate for those delays, estimation of future values is necessary. It has been found that a control algorithm using a synchronous rotating reference frame for each harmonic component is useful. This approach has been applied in a similar way in [16].

By transforming three-phase variables into a synchronous rotating reference frame, a reference frame that rotates with the same frequency as the three-phase signal, the resulting signal has a *dc*-component proportional to the fundamental component of the original signal. Even though there is much calculation power required to perform this transformation, it simplifies the control and should result in a more accurate cancellation of harmonic current.



In the first part of this chapter, the theory of the various transformations is shown. Then, the transformations are applied to distorted current signals to show the advantage of such transformations. Lastly, it is shown how the reference theory can be used to control an inverter to generate a desired output voltage.

## 2.2. Transformations

### 2.2.1. Stationary Reference Frame

In this research, a power invariant transformation has been chosen according to [17] which is used for the *pq-theory*. It transforms the three-phase variables  $f_a$ ,  $f_b$ , and  $f_c$  into an orthogonal two axis stationary reference frame with the components  $f_d$  and  $f_q$ . The transformation including the zero sequence component  $f_0$  is given by:

$$\begin{bmatrix} f_d^s \\ f_q^s \\ f_0^s \end{bmatrix} = \sqrt{\frac{2}{3}} \begin{bmatrix} 1 & -\frac{1}{2} & -\frac{1}{2} \\ 0 & \frac{\sqrt{3}}{2} & -\frac{\sqrt{3}}{2} \\ \frac{1}{\sqrt{2}} & \frac{1}{\sqrt{2}} & \frac{1}{\sqrt{2}} \end{bmatrix} \begin{bmatrix} f_a \\ f_b \\ f_c \end{bmatrix} \quad (2.1)$$

where the symbol  $f = f(t)$  represents voltage,  $v$ , or current,  $i$ . The superscript  $s$  is used to show that the variables are in the stationary reference frame. In motor theory, an additional subscript  $s$  or  $r$  is used to indicate if the variable is viewed from the stator or the rotor side of a machine. For simplification, this has been neglected in this document. The inverse transformation, the transformation from the stationary reference frame back into the three-phase variables is given by:

$$\begin{bmatrix} f_a \\ f_b \\ f_c \end{bmatrix} = \sqrt{\frac{2}{3}} \begin{bmatrix} 1 & 0 & \frac{1}{\sqrt{2}} \\ -\frac{1}{2} & \frac{\sqrt{3}}{2} & \frac{1}{\sqrt{2}} \\ -\frac{1}{2} & -\frac{\sqrt{3}}{2} & \frac{1}{\sqrt{2}} \end{bmatrix} \begin{bmatrix} f_d^s \\ f_q^s \\ f_0^s \end{bmatrix} \quad (2.2)$$

Since it is assumed that the three-phase three-wire system analyzed in this research is balanced (and contains no neutral current), the zero sequence component  $f_0^s = 0$ . Therefore (2.1) can be reduced to:

$$\mathbf{f}^s = \mathbf{K}^s \mathbf{f} \quad (2.3)$$

where

$$\begin{aligned}\mathbf{f} &= [f_a \ f_b \ f_c]^T \\ \mathbf{f}^s &= [f_d^s \ f_q^s]^T \\ \mathbf{K}^s &= \sqrt{\frac{2}{3}} \begin{bmatrix} 1 & -\frac{1}{2} & -\frac{1}{2} \\ 0 & -\frac{\sqrt{3}}{2} & \frac{\sqrt{3}}{2} \end{bmatrix}\end{aligned}$$

The matrix  $\mathbf{K}^s$  is the transformation matrix for the three-phase variable to the stationary two axis reference frame. The inverse of this transformation is given by:

$$\mathbf{f} = \mathbf{K}'^s \mathbf{f}^s \quad (2.4)$$

where

$$\mathbf{K}'^s = \sqrt{\frac{2}{3}} \begin{bmatrix} 1 & 0 \\ -\frac{1}{2} & \frac{\sqrt{3}}{2} \\ -\frac{1}{2} & -\frac{\sqrt{3}}{2} \end{bmatrix} \quad (2.5)$$

Using line-to-line voltages, the transformation can be written as:

$$\begin{aligned}v_d^s &= \sqrt{\frac{2}{3}}(v_{ab} - v_{ca}) \\ v_q^s &= \sqrt{\frac{1}{2}}v_{bc}\end{aligned} \quad (2.6)$$

For hardware implementation, only two measurements are taken, either two line currents or two line-to-line voltages. This simplification can be done since for a balanced system  $i_a + i_b + i_c = 0$  and  $v_{ab} + v_{bc} + v_{ca} = 0$ . In this case the transformation results in:

$$\begin{aligned}i_d^s &= \sqrt{\frac{2}{3}}i_a \\ i_q^s &= \sqrt{\frac{1}{2}}(i_a + \frac{3}{2}i_b)\end{aligned} \quad (2.7)$$

or

$$\begin{aligned}v_d^s &= \sqrt{\frac{2}{3}}(2v_{ab} + v_{bc}) \\ v_q^s &= \sqrt{\frac{1}{2}}v_{bc}\end{aligned} \quad (2.8)$$

### 2.2.2. Rotating Reference Frame

In a second step, the variables in the stationary reference frame are transformed into a rotating reference frame. For each harmonic, a separate reference frame rotating with its own frequency has to be generated. The transformation for the fundamental frequency is given by:

$$\mathbf{f}^e = \mathbf{K}^e \mathbf{f}^s \quad (2.9)$$

where

$$\begin{aligned} \mathbf{f}^e &= [f_d^e \ f_q^e]^T \\ \mathbf{K}^e &= \begin{bmatrix} \cos \theta_e & \sin \theta_e \\ -\sin \theta_e & \cos \theta_e \end{bmatrix} \\ \theta_e &= \int_0^t \omega_e dt + \theta_{e0} \end{aligned} \quad (2.10)$$

The superscript  $^e$  in  $\mathbf{K}^e$  and  $\mathbf{f}^e$  denotes that the reference frame is rotating with synchronous speed  $\omega_e = 2 * \pi f_s$  where  $f_s$  is the source frequency, i. e.  $f_s = 60Hz$ . The transformations for the harmonic frequencies into their corresponding rotating reference frames are defined in the same manner as for the fundamental in (2.9). The matrices  $\mathbf{K}^{-5e}$ ,  $\mathbf{K}^{7e}$ ,  $\mathbf{K}^{-11e}$ , and  $\mathbf{K}^{13e}$  refer to a rotating axis system synchronous with the 5<sup>th</sup>, 7<sup>th</sup>, 11<sup>th</sup> and 13<sup>th</sup> harmonics, i. e.  $\omega_{-5e} = -5\omega_e$ ,  $\omega_{7e} = 7\omega_e$ , and so on. The negative signs take into account that some frequencies (5<sup>th</sup>, 11<sup>th</sup>, etc.) result in negative rotating sequences, i. e. the vectors of those frequencies rotate in the opposite direction to those of the fundamental frequency.

The vector and matrix notation of the reference frame theory is used in the simulation since the used simulation tools as well the *DSP* do not allow the use of complex notations. Some of the operations can be more easily shown by using the complex vector form. Equation (2.9) can be rewritten as:

$$\underline{f}^e = \underline{f}^s e^{-j\theta_e} \quad (2.11)$$

where

$$\underline{f}^e = f_d^e + jf_q^e$$

$$\underline{f}^s = f_d^s + jf_q^s$$

Both notations are used interchangeably in this document as appropriate.

### 2.2.3. pq-Transformation

The *pq*-transformation or *instantaneous reactive power transformation* is a more specific transformation that uses the idea of the previous transformations [18]. In the first step, the phase voltage  $v_t$ , and load current currents  $i_r$  (Fig. 1.2) are transformed according to (2.3):

$$\mathbf{v}_t^s = \mathbf{K}^s \mathbf{v}_t \quad (2.12)$$

$$\mathbf{i}_r^s = \mathbf{K}^s \mathbf{i}_r \quad (2.13)$$

Instead of transforming both signals with a rotating reference frame, the two signals are used for a further transformation:

$$\begin{bmatrix} p \\ q \end{bmatrix} = \begin{bmatrix} v_d^s & v_q^s \\ -v_q^s & v_d^s \end{bmatrix} \mathbf{i}_r^s \quad (2.14)$$

where  $p$  is defined as the *instantaneous real power* and  $q$  as the *instantaneous reactive power*. More details about this transformation and the meaning of the  $p$  and  $q$  components can be found in [15].

If the voltage  $\mathbf{v}_t$  used for the transformation in (2.14) were purely sinusoidal, the *pq*-transformation would be equivalent to a transformation in a synchronous rotating reference frame. This has the advantage that no reference frame generator would have to be implemented since it could be generated directly from  $\mathbf{v}_t$ . Not generating a reference frame would save an immense amount of calculation power. Unfortunately, the voltage  $\mathbf{v}_t$  is not purely sinusoidal due to nonlinear loads in the power system. The harmonic

content in the voltage would produce additional distortion in the  $pq$ -transformation that could significantly reduce the ability to extract the harmonics in the current  $\mathbf{i}_r$ .

#### 2.2.4. Transformation of Harmonic Current

Because of the periodicity of the distorted current signals, the currents can be expressed in terms of a Fourier series. The sequence even can be simplified due to the assumption of a balanced system. The line currents can be decomposed as:

$$\begin{aligned} i_{ra} &= i_{ra}(t) = \sum_l i_{ra,l} = \sum_l \sqrt{2} I_{r,l} \cos l(\omega_e t - \varphi_l) \\ i_{rb} &= i_{rb}(t) = \sum_l i_{rb,l} = \sum_l \sqrt{2} I_{r,l} \cos l(\omega_e t - \varphi_l - \frac{2\pi}{3}) \\ i_{rc} &= i_{rc}(t) = \sum_l i_{rc,l} = \sum_l \sqrt{2} I_{r,l} \cos l(\omega_e t - \varphi_l + \frac{2\pi}{3}) \end{aligned} \quad (2.15)$$

with the harmonic number,  $l$ <sup>1</sup>, the *rms*-value of the harmonic current component,  $I_h$ , and the harmonic specific phase shift,  $\varphi_h$ . The line current,  $\mathbf{i}_r$ , transformed to the stationary reference frame results in:

$$\underline{i}_r^s = \underline{i}_r^s(t) = \sum_l \underline{i}_{r,l}^s \quad (2.16)$$

with

$$\underline{i}_{r,l}^s = \begin{cases} \sqrt{3} I_{r,l} e^{jl(\omega_e t - \varphi_l)} & \text{if } l = 1, 7, 13, \dots \\ \sqrt{3} I_{r,l} e^{-jl(\omega_e t - \varphi_l)} & \text{if } l = 5, 11, \dots \end{cases} \quad (2.17)$$

$\underline{i}_r^s$  transformed to the rotating reference frame  $\mathbf{K}^e$ :

$$\underline{i}_r^e = \underline{i}_r^e(t) = \sum_l \underline{i}_{r,l}^e \quad (2.18)$$

with

$$\underline{i}_{r,l}^e = \begin{cases} \sqrt{3} I_{r,l} e^{j\varphi_1} & \text{if } l = 1 \\ \sqrt{3} I_{r,l} e^{j((l-1)\omega_e t - l\varphi_l)} & \text{if } l = 7, 13, \dots \\ \sqrt{3} I_{r,l} e^{-j((l+1)h\omega_e t - l\varphi_l)} & \text{if } l = 5, 11, \dots \end{cases} \quad (2.19)$$

---

<sup>1</sup> $l$  includes all spectral components (fundamental and harmonics), i.e  $l = 1, 5, 7, 11, 13, \dots$ . On the other hand,  $h$  is used to only describe the harmonic without the fundamental components, i. e.  $h = 5, 7, 11, 13, \dots$

(2.19) shows that the fundamental current component,  $i_{r,1}$ , is transformed into a constant, non-oscillating value whereas the  $l$ -th harmonic component results in frequencies of  $(l+1)\omega_e$  or  $(l-1)\omega_e$ . By applying a low pass filter on  $i_r^e$ , the fundamental component can be extracted. If a reference frame rotating synchronous to one harmonic frequency is applied on  $i_r^s$ , this harmonic component results in a constant value and can be extracted by low pass filtering.

### 2.3. Space Vector Pulse Width Modulation

The theory of the reference frames is not only used for analyzing input signals of the system and extracting certain signal components, it also can be used to control the output stage, the inverter. The so called *Space Vector Pulse Width Modulation* (*SVPWM*) is used to control the inverter switches [19] for this project (Fig 2.1).

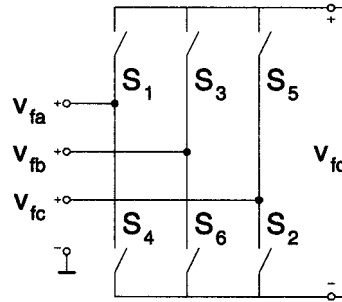


FIGURE 2.1: Inverter bridge used for active filter.

Neglecting the dead time control, there is always one switch open and one switch closed at the same time on a leg resulting in  $2^3 = 8$  switching combinations ( Fig. 2.2). Each combination results in a basic voltage vector (1) ... (8) when transformed to stationary reference frame as shown in Tab. 2.1. Vector (7) and (8) are zero vectors, i. e. the resulting output voltage is zero.

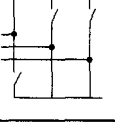
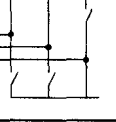
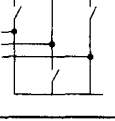
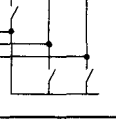
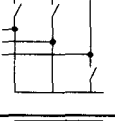
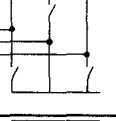
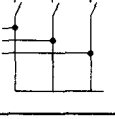
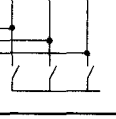
1		$\underline{v}_{f,(1)}^s = \sqrt{\frac{2}{3}} v_{fd} e^{j0}$	2		$\underline{v}_{f,(2)}^s = \sqrt{\frac{2}{3}} v_{fd} e^{j\frac{\pi}{3}}$
3		$\underline{v}_{f,(3)}^s = \sqrt{\frac{2}{3}} v_{fd} e^{j\frac{2\pi}{3}}$	4		$\underline{v}_{f,(4)}^s = \sqrt{\frac{2}{3}} v_{fd} e^{j\pi}$
5		$\underline{v}_{f,(5)}^s = \sqrt{\frac{2}{3}} v_{fd} e^{j\frac{4\pi}{3}}$	6		$\underline{v}_{f,(6)}^s = \sqrt{\frac{2}{3}} v_{fd} e^{j\frac{5\pi}{3}}$
7		$\underline{v}_{f,(7)}^s = 0$	8		$\underline{v}_{f,(8)}^s = 0$

TABLE 2.1: Inverter switching combination and corresponding output voltage.

In order to approximate an arbitrary output voltage, a combination of these eight voltage vectors are used and weighted over one switching interval according to (2.20) [20].

$$\overline{\underline{v}}_f^s = \frac{T_x}{T_p} \underline{v}_{f,(x)}^s + \frac{T_y}{T_p} \underline{v}_{f,(y)}^s + \frac{T_0}{T_p} \underline{v}_{f,(z)}^s \quad (2.20)$$

where  $T_0$  is given by  $T_p - T_x - T_y$  and where  $T_p$  is the total period (or PWM carrier period).  $T_x$  and  $T_y$  are times where the basic voltage vectors  $\underline{v}_{f,(x)}^s$  and  $\underline{v}_{f,(y)}^s$ , adjacent to  $\overline{\underline{v}}_f^s$ , are active.  $T_0$  is the time when either of the zero vectors  $\underline{v}_{f,(7)}^s$  or  $\underline{v}_{f,(8)}^s$  are active.

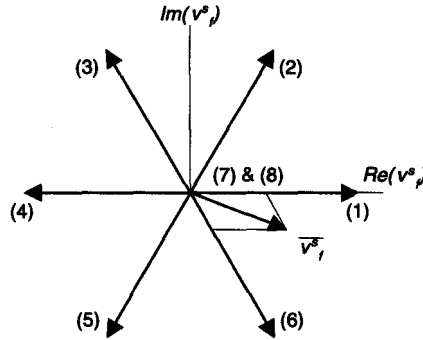


FIGURE 2.2: The eight voltage vectors characterizing the inverter operation.

For this research project, a symmetric PWM has been chosen, i. e. the carrier signal has a triangle shape with a period of  $T_p$  which also corresponds to the sampling frequency of the system  $T_s$ . Because of the symmetrical PWM, each switch that is involved in a switching sequence changes its state twice during a switching interval, i. e. the average switching frequency is equal to the carrier frequency. To compose the voltage vector  $\mathbf{v}_f^s$  shown in Fig. 2.2, the switching sequence (7)-(1)-(6)-(1)-(7) or (8)-(6)-(1)-(6)-(8) would have to be applied.

For the application, it has been chosen to start and end a switching sequence with the vector (8). An example of a switching pattern to create a vector in sector 6 (vector  $\bar{v}_f^s$  in Fig. 2.2) is shown in Fig. 2.3. Since a symmetrical triangular signal is used as carrier waveform, a symmetrical space vector *PWM* pattern is generated.

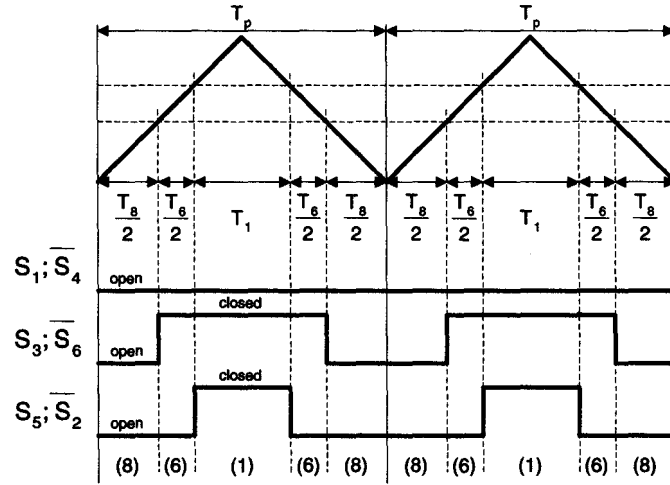


FIGURE 2.3: Symmetric space vector *PWM* waveform.



### 3. ELECTRICAL SYSTEM

#### 3.1. Introduction

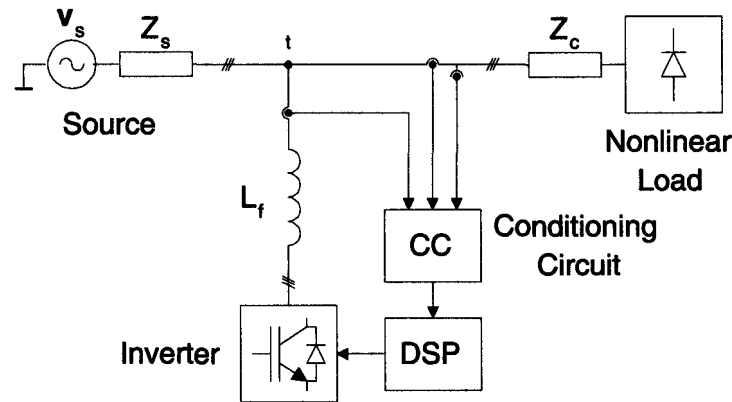


FIGURE 3.1: Block diagram of the hardware.

The electrical system can be divided in three main parts, the power system, the control circuit and the interface circuit between the power and control circuit (Fig. 3.1).

Assumptions are made for the system parameters which are used for the simulation. Unfortunately, it is not possible to exactly reproduce the hardware circuit. Parameters such as transfer functions of the current and voltage transducers were not available and could not be measured to complete satisfaction. Other parameters could not be included in the simulation since they would tremendously increase the complexity of the simulation resulting in a long calculation time. Therefore, the propagation delays of *AD*-converters and driving circuits for the power switches are neglected. It is also assumed that the circuit is piece-wise linear, i. e. the circuit behaves linearly between two switching states. Some parameter combinations resulted in convergence problems

and had therefore to be altered slightly. The results shown in this chapter are derived from simulations in *SIMULINK* using *PLECS*.

### 3.2. Power Circuit

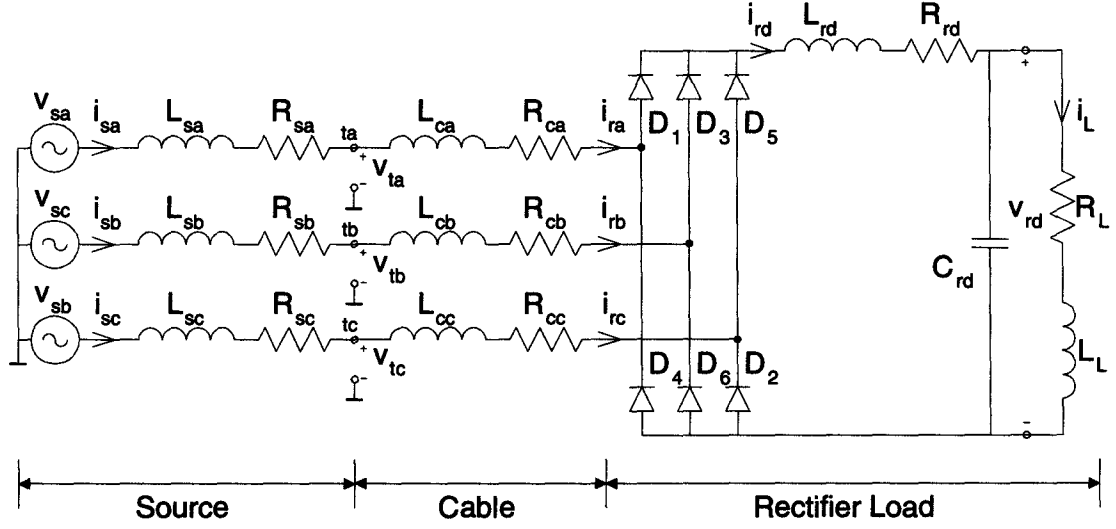


FIGURE 3.2: Load and source configuration.

The power circuit can be divided into three main parts, the source, nonlinear load and the active filter (Fig. 3.2). The circuit is analyzed without the active filter to show the dimensions of the distortion. The need for a switching ripple filter and its characteristic is also demonstrated. A detailed schematic of the total circuit is given in Appendix C.

It is worth noting that the simulations have been performed on a 460V-system, a widely used industrial voltage rating to drive three-phase power loads. For the hardware implementation, it was decided to test the circuit on a 230V-system to gain a larger safety margin for the power electronic devices.

### 3.2.1. Source and Load

The complete three-phase circuit diagram is shown in Fig. 3.2. The source consists of an ideal three-phase voltage source,  $\mathbf{v}_s$  and a source impedance  $R_s$  in series with a source inductance  $L_s$ . The terminal voltage of the source is denoted as  $\mathbf{v}_t$ . This is also the coupling point,  $t$ , of the active filter. The source is assumed to be an ideal voltage source  $V_{s,LL} = 460V$  connected through a transformer rated at  $500kVA$  with a impedance of 4% and an efficiency of 98%.

Between the source terminals,  $t$ , and the rectifier, a 100ft long, 14 AWG cable is approximated (for a  $5kVA$  load) with the series resistance  $R_s$  and inductance  $L_s$ .

The nonlinear load is represented by a rectifier with a  $dc$ -link inductor  $L_{rd}$  including losses  $R_{rd}$ , filtering capacitor  $C_{rd}$ , and a load consisting of  $R_L$  and  $L_L$ . The rectifier is designed to supply  $P_L \simeq 5kW$  with a voltage ripple of  $V_{rd,ripp} = 1\% - 2\%$ . Even though the  $dc$ -link inductor has not been included in the design of the rectifier, convergent problems in the simulation could be reduced by assigning some arbitrary small

Parameter	calculated value	simulation value
$V_{s,LL}$	460V	460V
$R_s$	4.2m $\Omega$	4.2m $\Omega$
$L_s$	44.9 $\mu H$	44.9 $\mu H$
$R_c$	1.96 $\Omega$	0.5 $\Omega$
$L_c$	118 $\mu H$	118 $\mu H$
$R_{rd}$	—	0.1 $\Omega$
$L_{rd}$	—	1 $\mu H$
$R_L$	—	80 $\Omega$
$L_L$	—	1 $\mu H$
$C_{rd}$	—	2.5mF

TABLE 3.1: Simulation parameters.

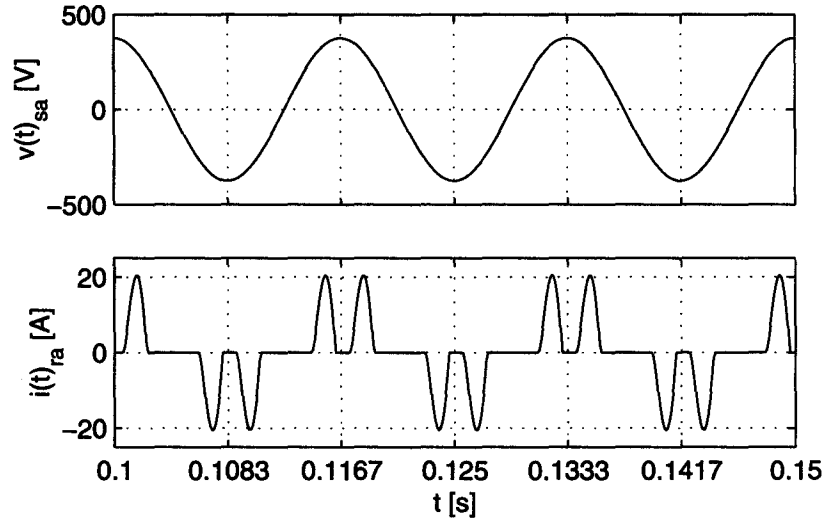


FIGURE 3.3: Source voltage  $v_{sa}$  and load current  $i_{ra}$ .

value. The parameter values on the  $dc$ -side are chosen through simulation iterations until the specifications for the load power and voltage ripple were met. The final system parameters can be found in Tab. 3.1 and the resulting load power and  $dc$ -voltage ripple in Tab. 3.2.

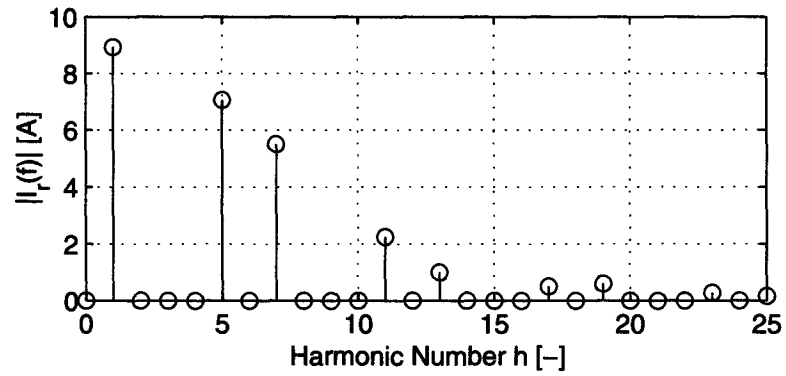
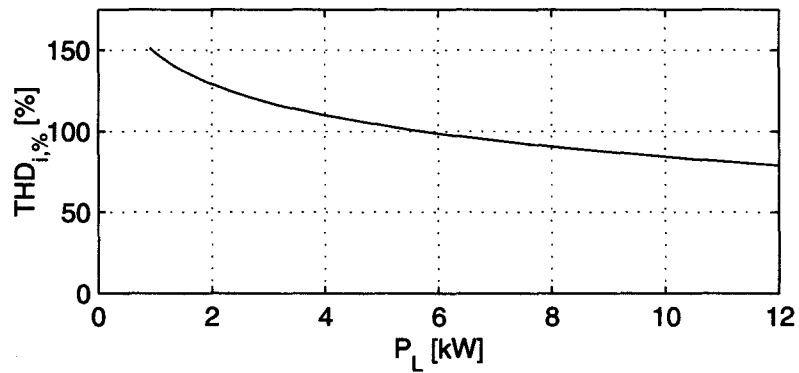


FIGURE 3.4: Spectrum of load current  $i_{ra}$ .

Parameter	Simulated Value	
$I_{r,1}$	6.32A	100%
$I_{r,5}$	5.00A	79.1%
$I_{r,7}$	3.89A	61.6%
$I_{r,11}$	1.59A	25.2%
$I_{r,13}$	0.71A	11.2%
$THD_{i_r}$	104.5%	
$P_L$	4878W	
$V_{rd}$	624V	
$V_{rd,ripp}$	1.37%	

TABLE 3.2: Simulation results.

Fig. 3.3 shows the simulated waveforms using the circuit and parameters described above. As can be seen, the load current  $i_{ra}$  is highly distorted. The spectrum of the load current is shown in Fig. 3.4. A more qualitative listing of the current and voltage distortion is given in Tab. 3.2. Refer to Appendix A for more details on how the spectra are determined.

FIGURE 3.5: Total harmonic distortion  $THD_{i_r}$  under different load conditions.

The current distortion in Fig. 3.3 is due to the discontinuous conduction of the rectifier diodes resulting in the characteristic "double-hump" current waveform. The shorter the conducting time, the higher the distortion. For a given system designed for rated load, the conduction time varies according to the applied load (Fig. 3.5). It can be seen that the distortion factor increases if smaller loads are applied.

### 3.2.2. Active Filter Circuit

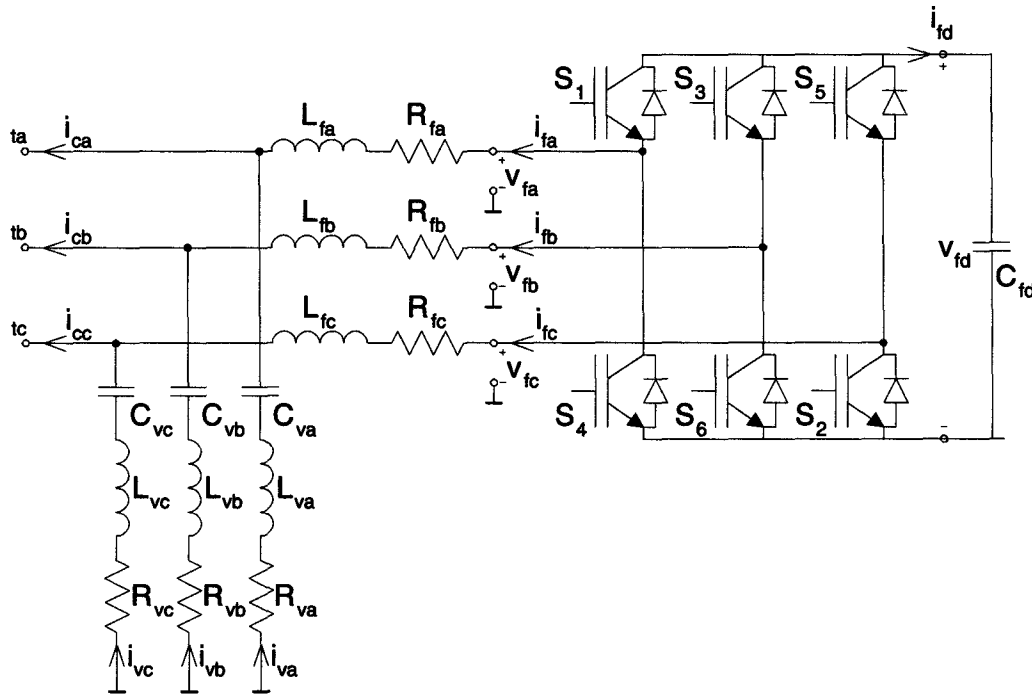


FIGURE 3.6: Active filter circuit with switching ripple filter.

Fig. 3.6 shows the active filter circuit that is connected in parallel at the source terminals (point  $t$  in Fig. 3.2). The active filter consists of an inverter coupled with series inductors  $L_f$  (including losses  $R_f$ ) to the power line and a switching ripple filter  $C_v$ - $L_v$ - $R_v$ .

The inverter is built with six Insulated Gate Bipolar Transistors (*IGBTs*) with free-wheeling diodes. For the simulation, the *IGBTs* are replaced with ideal switches. Since it is possible in simulation to turn on and off two switches instantaneously, there is no need for the free-wheeling diodes.

The *dc*-bus capacitor  $C_{fd}$  has not yet been included in the project. Instead, the capacitor is replaced with a constant *dc*-source  $V_{fd}$ . In the future, the capacitor should be fed from the power source  $v_s$  and charged with a constant voltage which would require an additional control loop. The active filter should neither absorb a significant amount of energy from the system nor inject energy to the system. In the case of a *dc*-source, the source would have to compensate for losses in the inverter system. In the case of the *dc*-capacitor, the losses would have to be compensated with energy from the power source  $\mathbf{v}_s$ .

Parameter	Simulation Value
$V_{fd}$	800V
$R_f$	1 $\Omega$
$L_f$	1mH
$R_v$	0.5 $\Omega$
$L_v$	31.08 $\mu$ H
$C_v$	13.82 $\mu$ F

TABLE 3.3: Simulation parameters for active filter.

The filter output voltage is denoted as  $\mathbf{v}_f$ , the filter current as  $\mathbf{i}_f$ , the switching ripple filter current as  $\mathbf{i}_v$ , and the compensation current as  $\mathbf{i}_c$ . The circuit parameter values are listed in Tab. 3.3. The *dc*-bus voltage  $V_{fd} = 800V$  has been chosen rather high in order to not limit the compensation ability of the active filter. A high *dc*-bus voltage results in high current ripple in  $\mathbf{i}_f$  which is not desired. In the future, when

the  $dc$ -bus voltage source is replaced with a  $dc$ -capacitor, the voltage should be reduced significantly since it has to be fed from the grid. If all switches are off, the inverter bridge acts as a three-phase rectifier and can charge the  $dc$ -bus to a maximum voltage of about  $\sqrt{2}V_{s,LL} = 650V$ . The control algorithm for the switches would then have to boost the voltage in order to serve as an inverter for the active filter to the required voltage for the active filter mode.

### 3.2.3. Switching Ripple Filter

Because of the switching nature of the inverter, high current ripple is present [21]. Fortunately, the ripple has a fundamental frequency equal to the switching frequency  $f_p = f_s = 7680Hz$  which is easier to filter than low frequencies. In order to filter the current, a switching ripple filter (*SRF*) is connected in parallel to the active filter consisting of a series  $L$ - $C$ - $R$  band-pass filter. The filter is designed with a resonant frequency  $f_0 = f_p = 7680Hz$  to achieve minimum impedance at the fundamental frequency of the switching ripple and a quality factor of  $Q = 3$  to dampen the resonant circuit. The impedance of the filter is given in (3.1) and its frequency response is shown in Fig. 3.7.

$$Z_v(s) = \frac{1 + sR_vC_v + s^2L_vC_v}{sC_v} \quad (3.1)$$

As can be seen in the frequency response of the filter, the impedance for the fundamental line frequency is finite, i.e  $Z_v(j2\pi60) = 192\Omega\angle -89.8^\circ$ . This low impedance results in a fundamental current  $|I_{v,1}| = 1.64A$  that changes either the power factor of the system or has to be compensated for by the active filter.

For the fundamental frequency of the switching ripple, the impedance of the filter is  $Z_v(j2\pi7680) = 0.5\Omega\angle 0^\circ$ . This non-zero impedance does not totally absorb the switching ripple. The filtering performance also depends on the source impedance  $Z_s(s)$  and load impedance. The source and load impedances have to be large compared to the switching ripple filter impedance at the switching frequency in order to achieve good suppression of switching ripple in the load current.



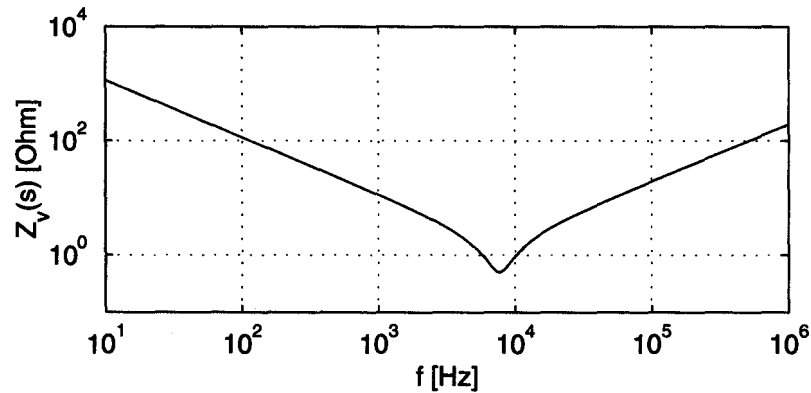


FIGURE 3.7: Frequency response of switching filter ripple  $Z_v(j\omega)$ .

### 3.3. DSP Interface

To satisfy the tremendous calculation need for the active filter, a *DSP* is used to implement the active filter algorithm. The center of the hardware is a *TMS320C240 DSP Controllers Evaluation Module* with the following main features:

- 16 bit fixed-point arithmetic core unit
- 20 MIPS
- 544 words of internal dual access RAM
- 128k words of external on-board SRAM
- Dual 10-bit, 8-channel analog-to-digital converters (ADCs)
- 12 PWM channels including dead time generator
- 4-channel, 12-bit on-board digital-to-analog converters

The *DSP* is programmed in assembler language to use the full capabilities of its hardware performance and to prevent loss of calculation power by program overhead resulting from the use of a high level language. Because it is a 16 bit fixed-point unit, the program has to be carefully designed such that the quantization errors do not become significant and cause malfunctions of the program.

To interface the DSP with the power circuit, signal conditioning and protection circuitry is built. A detailed description of the hardware circuit can be found in [13]. The next two sections describe the function of the interface circuit in a block diagram manner.

### 3.3.1. Interface Circuits

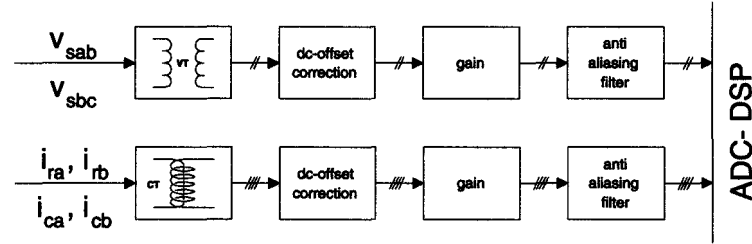


FIGURE 3.8: Block diagram of input interface circuit.

Six signals are measured and interfaced with the *DSP* as shown in Fig. 3.8. Two load currents  $i_{ra}, i_{rb}$  and two compensation currents  $i_{ca}, i_{cb}$  are measured with current transducers (*CT*) and two terminal voltages  $v_{tab}, v_{tbc}$  are measured with voltage transducers (*VT*) for electrical isolation. The voltage transducers have low pass characteristics with a cut off frequency well above the switching frequency, i. e. the whole signal spectrum can be measured. The same does not apply for the current transducers. The transfer function of the *CTs* have a band pass characteristic. Therefore, *dc*-components or even higher harmonics cannot be measured (there are no exact specifications for the *CTs*). The signals have to be offset-corrected and amplified to match the required signal level of the *DSP* of  $0V - 5V$ .

To reduce some aliasing, a second order filter is used with the frequency response shown in Fig. 3.9. The low filter order is used to prevent any additional stability

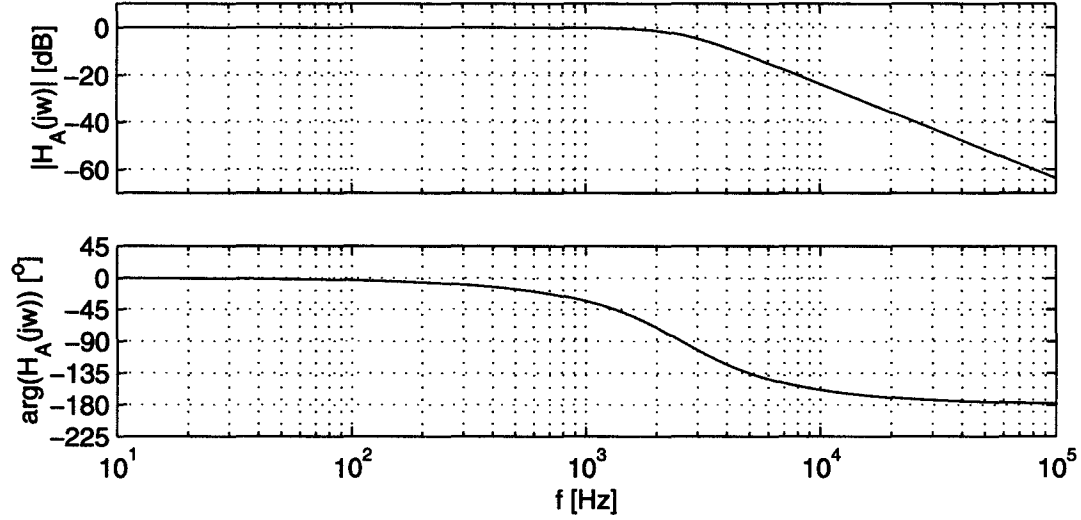


FIGURE 3.9: Frequency response of anti aliasing filter  $H_A(j\omega)$ .

problems in the closed loop control system. In addition, the highly distorted currents are pre-filtered by the low pass characteristic of the *CTs*. The *VTs* have a high enough bandwidth to pass frequencies even higher than the switching frequency, but the voltage distortion is low enough to be filtered only by the anti-aliasing filter.

The active filter has only 6 *PWM* output signals to control the inverter. Because of the requirement to build a flexible system, the output signals are passed through a programmable array logic (*PAL*). For this application, the *PAL* is not necessary. The logic signals are passed through opto-couplers for electric isolation between the control

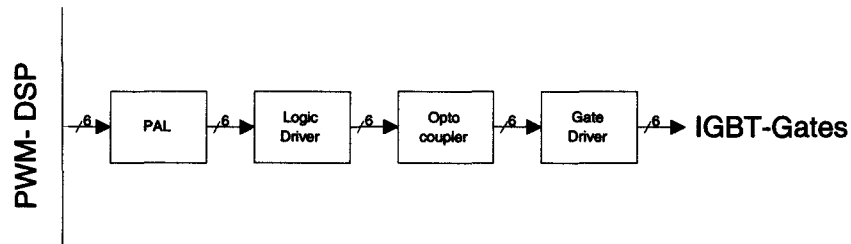


FIGURE 3.10: Block diagram of output interface circuit.

circuit and the power system. To drive the gates, each *IGBT* requires a separate drive logic including its own power supply.

### 3.3.2. Transfer Characteristic

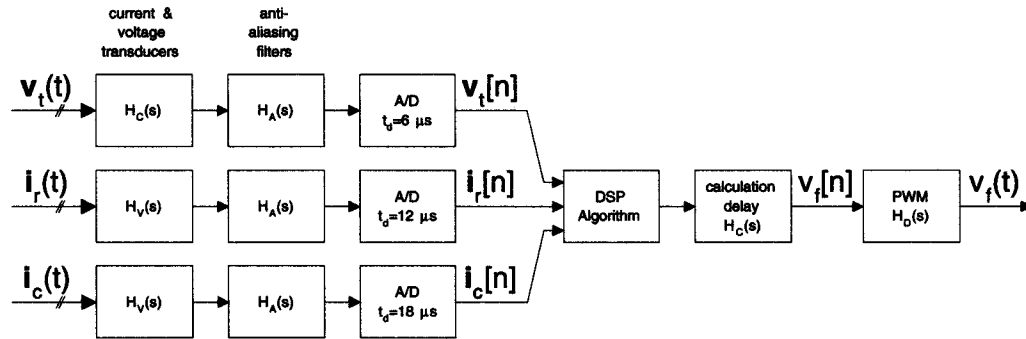


FIGURE 3.11: Block diagram control system.

The block diagram in Fig. 3.11 shows the transfer characteristic of the hardware system. As explained in the previous section, the input signals are passed through either voltage or current transducers with the transfer characteristic  $\underline{H}_C(s)$  and  $\underline{H}_V(s)$ , respectively. All signals are passed through an anti aliasing filter  $\underline{H}_A(s)$ .

The *DSP* is only capable of sampling two signals simultaneously, but the filter is implemented in a three-phase system. Since it is assumed that the power system is completely balanced, only two of the three signals are measured according to (2.7) and (2.8) and sampled simultaneously. The *AD*-converters require a minimum conversion time of  $t_d = 6\mu s$ , represented with  $\underline{H}_D$ . Therefore, the signal pairs are delayed by  $6\mu s$ ,  $12\mu s$  and  $18\mu s$ , respectively. Once all signals are sampled, the algorithm is processed within the *DSP*. The sampling and the calculations have to be performed within one sampling interval  $T_T = \frac{1}{7680Hz} = 130\mu s$ . The calculation delay is considered with  $\underline{H}_D = e^{-j\omega T_T}$ . The only output signals are the *PWM* patterns which control the *IGBTs*.

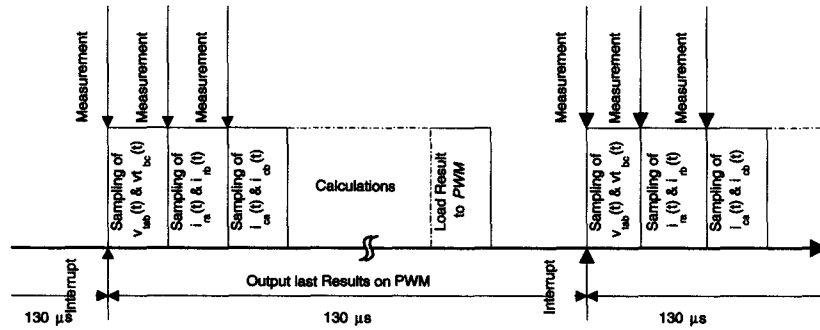


FIGURE 3.12: Timing diagram.

The new *PWM*-pattern is active during the following sampling interface, resulting in an additional delay of one sampling period. In the timing diagram (Fig. 3.12), only significant delays and filter characteristics are included. Minor propagation delays, wait-state delays, etc. are not included.

All the circuit elements are assumed to have a linear characteristic. With this assumption, the propagation and sample delays and transfer functions result in an additional phase shift or magnitude change of the sinusoidal signals. The delays have a tremendous effect in the filtering performance of the active filter as shown in the next chapter.

## 4. CONTROL SCHEME

### 4.1. Compensation with Ideal Hardware

#### 4.1.1. Compensation in Delayless System

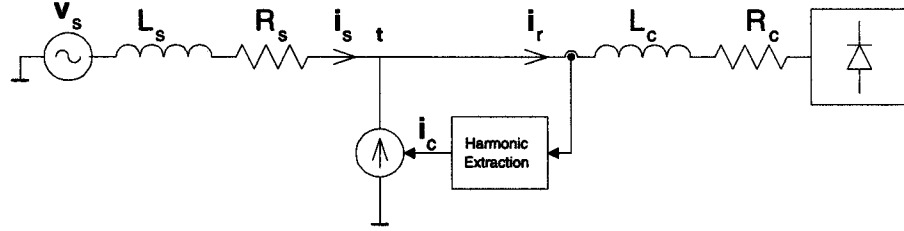


FIGURE 4.1: Ideal compensation principle.

Fig. 4.1 shows the basic idea of harmonic current compensation. The distorted load current,  $i_r$ , is measured and the fundamental component,  $i_{r,1}$ , is separated from the harmonic component,  $i_{r,h}$ . Ideally, the current source,  $i_c$ , injects current equal to the harmonic load current component but with opposite phase to effectively cancel the distortion resulting in undistorted source current  $i_s$ .

$$i_s = i_r - i_c = (i_{r,1} + i_{r,h}) - i_{r,h} = i_{r,1} \quad (4.1)$$

In order to separate the fundamental and harmonic current components, the load current is transformed to the reference frame which rotates with the fundamental frequency. By averaging (or low pass filtering) the transformed current  $i_r^e$ , the fundamental component  $\overline{i_r^e} = i_{r,1}^e$  can be extracted.

$$i_r^e = \overline{i_r^e} + \widetilde{i_r^e} = \underline{K^e} \underline{K^s} i_r = \underline{K^e} \underline{K^s} (i_{r,1} + i_{r,h}) \quad (4.2)$$

$$i_{r,1} = \underline{K^s} \underline{K^e} \overline{i_r^e} \quad (4.3)$$

$$\underline{i}_c = \underline{i}_{r,h} = \underline{i}_r - \underline{i}_{r,1} = \underline{K}^s \underline{K}^e \tilde{\underline{i}}_r^e \quad (4.4)$$

The resulting decomposed load current of the system proposed in Fig. 3.2 is shown in

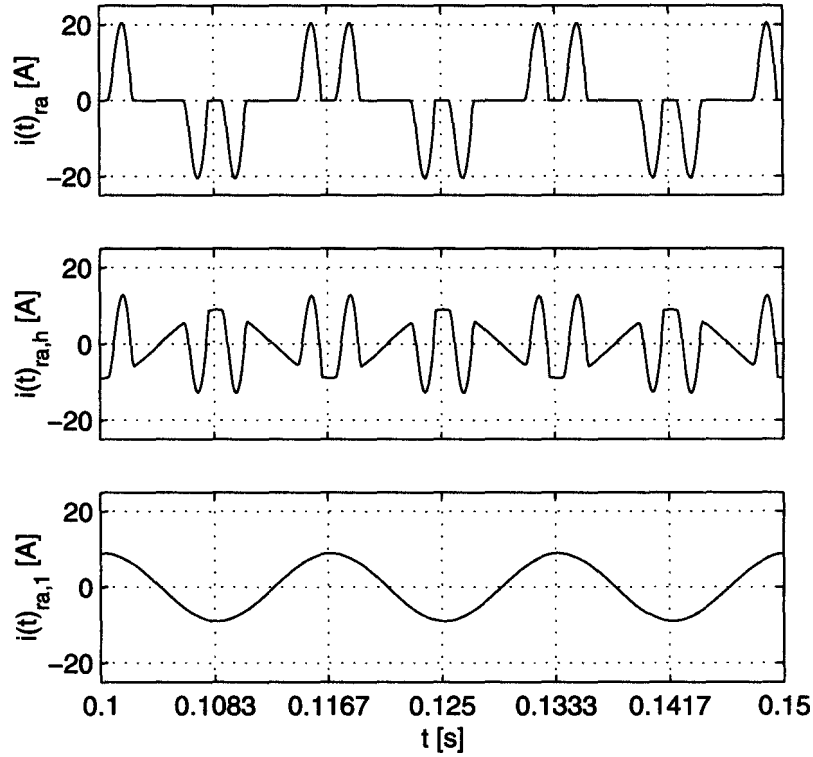


FIGURE 4.2: Separated fundamental and harmonic current.

Fig. 4.2. With ideal compensation, no harmonic current distortion would be left in the source current, i. e.  $\underline{i}_{s,h} = 0$ . There are some major factors that limit the ability to cancel harmonic currents as proposed above:

- An ideally controlled current source does not exist on the power system.
- There are system delays resulting in reduced cancellation for lower order harmonics or even amplification of higher order harmonics.

- There is some cancellation current flowing into the load causing an unwanted feedback loop. Since there might be significant delays present in the *DSP* system and the control algorithm, the loop could become unstable. If there is only a small amount of current flowing back to the load, the loop gain is small as well, and therefore, the loop is less likely to become unstable.

#### 4.1.2. Effects due to Delayed Current Injection

As shown above, major delays are caused by the calculation delay and the delay of the *PWM* controlled inverter. Adding up these delays, the total delay is at least  $t_d = 2T_T = 260\mu s$ . The delay results in the following phase shifts  $\varphi_d(t_d)$  of the fundamental and harmonic signals (Tab. 4.1):

$$\varphi_d(t_d) = 360^\circ l f_s t_d \text{ with } l = 1, 5, 7, 11, 13 \dots \quad (4.5)$$

k	$\varphi_d(T_s)$ [°]	$\varphi_d(2T_s)$ [°]
1	2.8	5.6
5	11.3	22.5
7	19.7	39.4
11	30.9	61.9
13	36.6	73.1

TABLE 4.1: Phase shift due to system delays of  $t_d = T_T$  and  $t_d = 2T_T$ .

The effects of delayed cancellation in the source current can be seen in Fig. 4.3. The figures have been created in an open loop simulation:

$$\underline{i}_s(t) = \underline{i}_r(t) - \underline{i}_c(t - t_d) \quad (4.6)$$



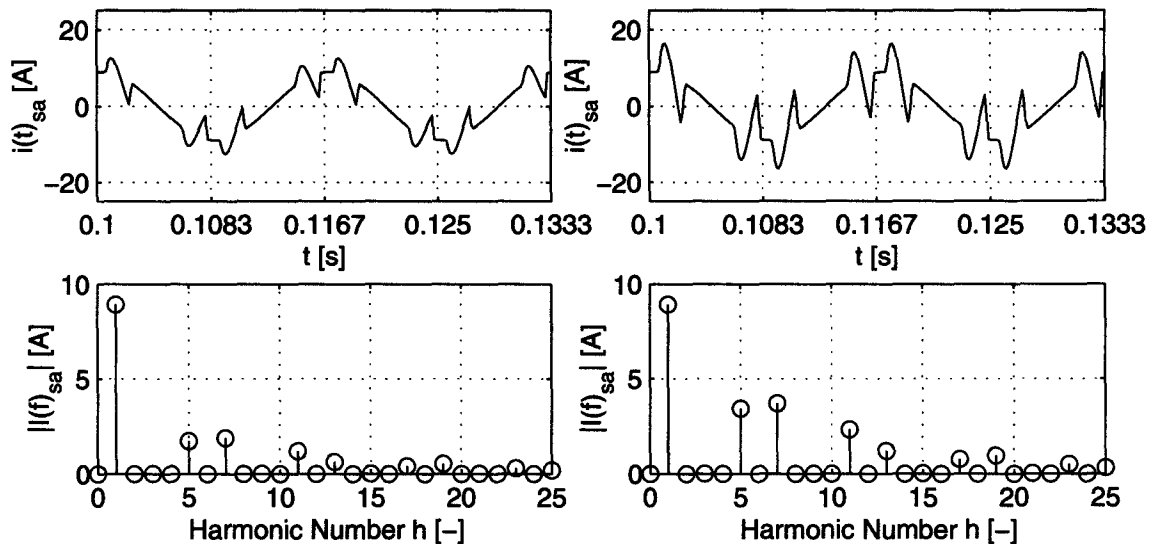


FIGURE 4.3: Effect on delayed compensation current injection  
(left:  $t_d = T_T$ , right:  $t_d = 2T_T$ ).

Since delays are inherent in a system using a *DSP*, solutions have to be found to compensate accordingly [22],[23]. The delays could be reduced by increasing the sampling and switching frequency of the active filter. An active filter with a sampling frequency  $f_T = 200kHz$  and a switching frequency  $f_p = 18kHz$  is proposed in [24].

In this research, another way to compensate for system delays is chosen. Each harmonic to be cancelled is separately extracted and its magnitude and phase determined. By knowing the magnitude and phase, future values of the compensation current can be estimated and therefore the compensation current matches the distortion with opposite phase.

## 4.2. Block Diagram

In order to study the control circuit for the active filter, it is necessary to discuss the effects of the output of the *DSP* (inverter) on the system and the inputs of the *DSP*. For that reason, two assumption are made:



the inverter bridge are open resulting in no current flow out of the inverter, i. e.  $\underline{i}_f = \underline{0}$ . Because of the assumptions made above, the source current results in:

$$\underline{i}_s = \underline{i}_r - \underline{i}_v - S\underline{i}_f \quad (4.8)$$

where

$$\underline{i}_f = \frac{\underline{v}_f - \underline{v}_t}{\underline{Z}_f}$$

$$\underline{i}_v = \frac{\underline{v}_t}{\underline{Z}_v}$$

### 4.3. Control Strategy

#### 4.3.1. Overview

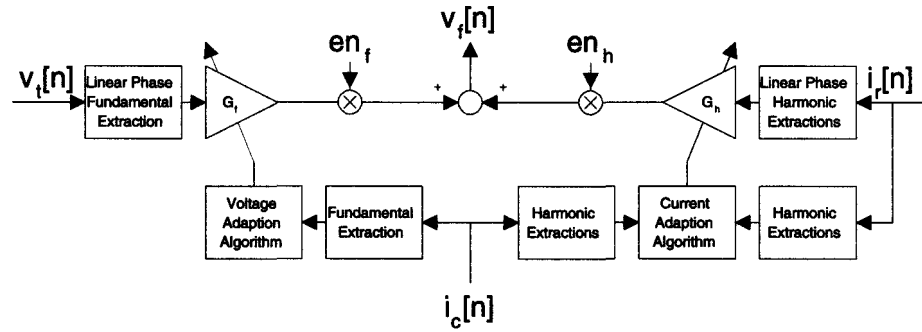


FIGURE 4.5: Control strategy overview.

Fig. 4.5 shows an overview of the proposed control strategy. The controller has to fulfill the following four tasks:

1. Control the fundamental component of the filter voltage,  $\underline{v}_{f,1}$ , by changing the fundamental correction factor,  $\underline{G}_f$ , in such a way that there is no fundamental filter current present, i. e.  $\underline{i}_{c,1} = 0$ .

2. Control the harmonic components of the filter voltage,  $\underline{v}_{f,h}$ , by changing the fundamental correction factor,  $\underline{G}_h$ , in such a way that the harmonic filter current equals the desired filter current, i. e.  $\underline{i}_{c,h}^* = \underline{i}_{r,h}$ .
3. Predict the desired filter current to compensate for system delays.
4. Adapt the parameters  $\underline{G}_h$  and  $\underline{G}_f$  of the prediction algorithm to compensate the slow drifting system parameters.

The switches  $en_f = \{0, 1\}$  and  $en_h = \{0, 1\}$  are used to enable and disable the fundamental and harmonic component output. If  $en_f = 0$ , output voltage is not present, i. e. all six switches of the inverter bridge are off as well.

In the following derivation of the control algorithm, the power system is assumed to be at steady state. Even though the adaption algorithm may change parameters over time, the adaption is slow in comparison to the dynamics of the power system such that a steady state assumption is valid for the electrical part of the system.

#### 4.3.2. Fundamental Control

The fundamental current control of the active filter is one of the key points of the control algorithm. The fundamental current is derived with

$$\underline{i}_{f,1} = \frac{\underline{v}_{f,1} - \underline{v}_{t,1}}{\underline{Z}_f} \quad (4.9)$$

In order to zero the fundamental filter current,  $\underline{i}_{f,1}$ , the fundamental filter voltage,  $\underline{v}_{f,1}$ , must be equal to the fundamental source terminal voltage,  $\underline{v}_{t,1}$ . Even the smallest phase shift between the two voltages due to system delays can result in damaging currents. A phase shift  $\varphi_{v_{t,1}-v_{f,1}} = 5.6^\circ$  (refer to Tab. 4.1) results in a fundamental current  $I_{f,1} = 69.8A$ .

Because of the sensor placement, the fundamental control algorithm does not minimize the filter current  $\underline{i}_{f,1}$ . Instead the compensation current  $\underline{i}_{c,1}$  is measured and

minimized:

$$\underline{i}_{c,1} = \underline{i}_{v,1} + \underline{i}_{f,1} = -\frac{\underline{v}_{t,1}}{\underline{Z}_v} + \frac{\underline{v}_{f,1} - \underline{v}_{t,1}}{\underline{Z}_f} \quad (4.10)$$

In order to set the current  $\underline{i}_{c,1} = 0$ , the following requirement can be derived from 4.10:

$$\underline{v}_{f,1} = \frac{\underline{Z}_v + \underline{Z}_f}{\underline{Z}_v} \underline{v}_{t,1} \quad (4.11)$$

The fundamental component of the output voltage,  $\underline{v}_{f,1}$ , is derived from the filtered terminal voltage transformed to the rotating reference frame  $K^e$

$$\underline{v}_f^{s''}[n] = (\underline{K}^e[n])^{-1} \underline{v}_f^{e''}[n] = (\underline{K}^e[n])^{-1} \underline{G}_f f_{fir}[n] * \underline{v}_t^e[n] = (\underline{K}^e[n])^{-1} \underline{G}_f f_{fir}[n] * \underline{K}^e[n] \underline{v}_t^s[n] \quad (4.12)$$

If the system is in steady state, (4.12) can be rewritten for the fundamental component assuming that the low pass filter blocks harmonic components

$$\underline{v}_{f,1}^{s''}[n] = \underline{G}_f \underline{v}_{t,1}^s[n] \rightarrow \underline{v}_{f,1}^{s''} = \underline{G}_f \underline{v}_{t,1}^s \quad (4.13)$$

Even though it is assumed that there is little or no distortion present in the terminal voltage,  $\underline{v}_t$ , the voltage is filtered with a linear phase filter  $f_{fir}$ . For the filter, a *FIR*-filter has been chosen with the frequency response shown in Fig. 4.7. Using a *FIR*-filter has two positive effects: first, the linear phase response of the filter results in a constant group delay of all frequency components. In the case where harmonic components are present, these components are only reduced in magnitude but undergo no change in phase shift in

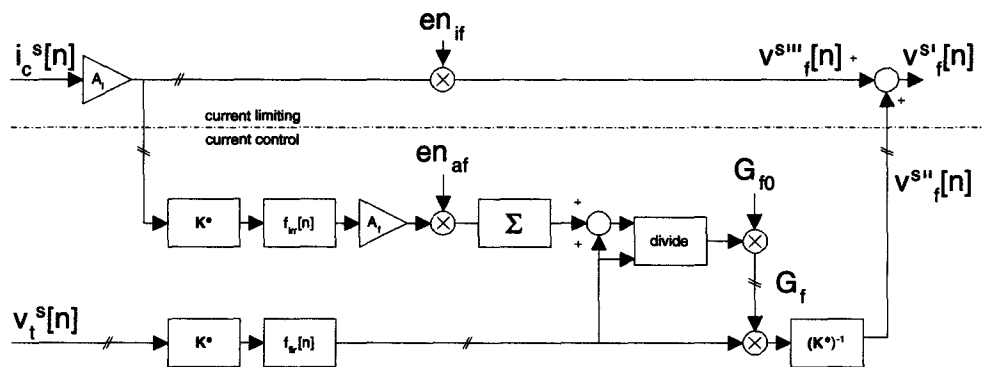


FIGURE 4.6: Control circuit for fundamental current.

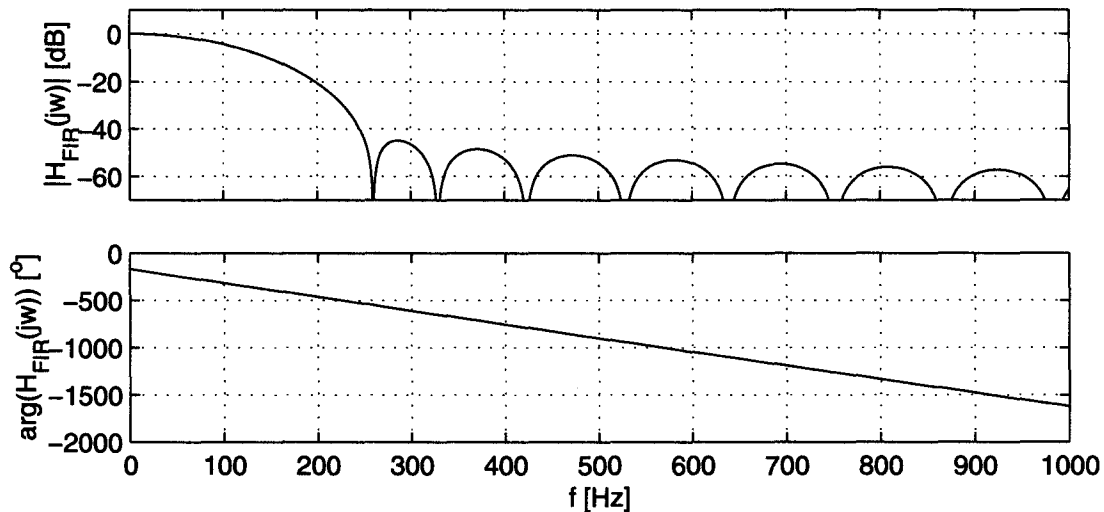


FIGURE 4.7: Bode-diagram of linear phase *FIR*-filter for fundamental and harmonic extraction.

relation to the fundamental signal component. This ensures that the system does not add harmonic signals with phase shift depending on the filter characteristics of  $f_{fir}$ . Second, the impulse response of the *FIR*-filter has a length of 64 samples which corresponds to the time of one half of a cycle of the fundamental period,  $T_s$ . In the case of a transient in the power system, the active filter should compensate correctly again after one half of a fundamental period. Both characteristics of the *FIR*-filter might be more significant in the case of the harmonic current controller than that of the fundamental voltage control. The drawback of using a *FIR*-filter is that it requires high computational power.

From the block diagram in Fig. 3.11 and Fig. 4.6 the overall transfer function of the fundamental components of  $\underline{v}_t$  and  $\underline{v}_f$  can be derived

$$\underline{v}_{f,1} = \underline{H}_P \underline{H}_D \underline{G}_f \underline{H}_C \underline{H}_A \underline{H}_V \underline{v}_{t,1} \quad (4.14)$$

where  $\underline{G}_f$  describes the transfer function of the *DSP* algorithm in the continuous time domain. All of the transfer functions are linear and change only the phase and magnitude of the sinusoidal signal, i. e.  $\underline{H} = \underline{H}(j\omega)$ .

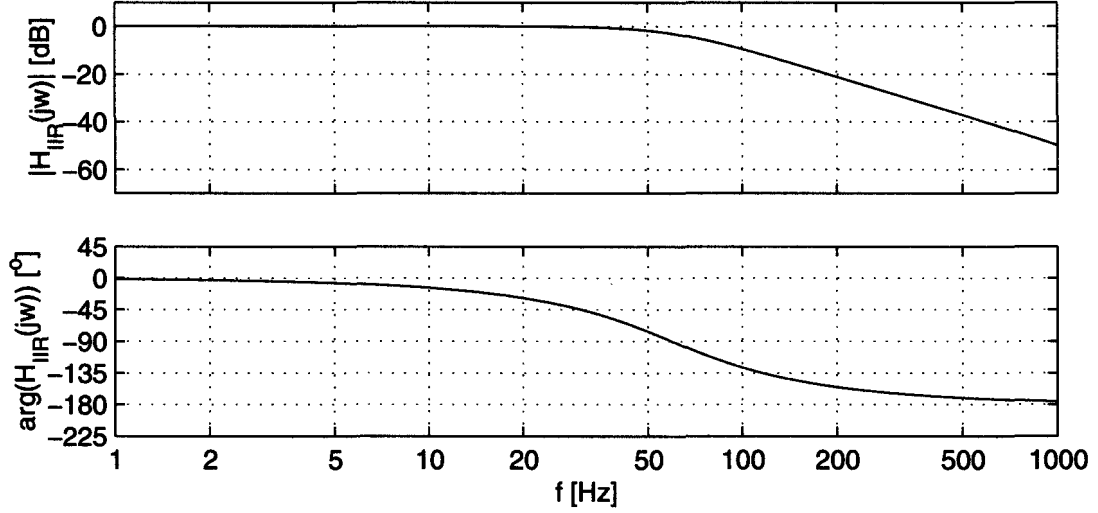


FIGURE 4.8: Bode-diagram of *IIR*-filter for adaption algorithm.

All the parameters in (4.11) and (4.14) are fixed except  $\underline{G}_f$ . In order that (4.14) satisfies the condition (4.11),  $\underline{G}_f$  must be set accordingly

$$\underline{G}_f = \frac{\underline{Z}_f + \underline{Z}_v}{\underline{Z}_v \underline{H}_P \underline{H}_D \underline{H}_C \underline{H}_A \underline{H}_V} \quad (4.15)$$

Since most system parameters are not exactly available, the algorithm starts with an initial guess of  $\underline{G}_f$ ,  $\underline{G}_{f0}$ , and adapts until the fundamental compensation current  $\underline{i}_{c,1}$  is zero or minimized. For an initial value, only the known and significant parts of (4.15) are incorporated, resulting in

$$\underline{G}_{f0} = \frac{1}{\underline{H}_P \underline{H}_D} = e^{j2\omega T_T} \quad (4.16)$$

Fig. 4.6 shows the current control part with adaption. The fundamental component of the compensation current is extracted by filtering the compensation current  $\underline{i}_c^e$

$$\underline{i}_{c,1}^e[n] = \overline{\underline{i}_{c,1}^e[n]} \approx \underline{i}_c^e[n] * f_{iir}[n] \quad (4.17)$$

Since there is no real requirement in the length of the impulse response nor in the phase response of the filter, a fourth order *IIR*-filter with low computational requirement has been chosen. The frequency response of the filter is shown in Fig. 4.8.

The error current (remaining fundamental current  $i_{c,1}$ ) is integrated in order to approach the ideal  $\underline{G}_f$ . The factor  $A_f$  determines the adaption speed. The value for  $A_f$  is derived experimentally to optimize speed and stability of the system. The adaption of  $\underline{G}_f$  can be enabled and disabled with the signal  $en_{af} = \{0, 1\}$ . This switch is used to disable the adaption during transients of the system.<sup>2</sup>

Because the initial parameter  $\underline{G}_{f0}$  may not be exact enough, the resulting phase shift between  $\underline{v}_{t,1}$  and  $\underline{v}_{v,1}$  could result in high compensation currents exceeding the ratings of the power system. In order to limit the current at start up, a current limiting loop consisting of an ordinary proportional controller is included. The parameter  $A_i$  is the proportional gain of the  $P$ -controller. This loop is only active ( $en_{if} = 1$ ) during startup of the circuit and at times when protection is needed to limit the current.<sup>3</sup>

The output of the fundamental controller  $\underline{v}_f^s$  adds to the output of the harmonic controller and is passed to the  $PWM$  controller.

#### 4.3.3. Harmonic Controller

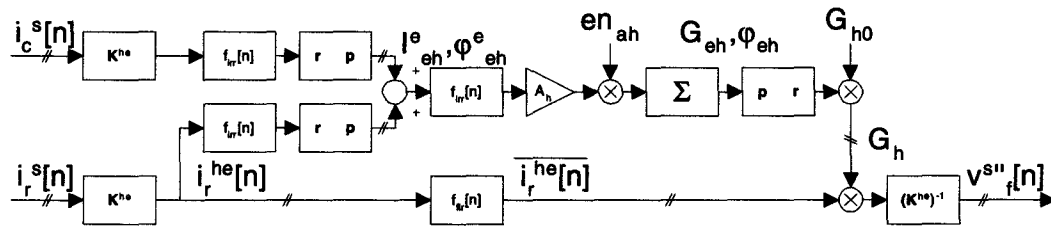


FIGURE 4.9: Control circuit for one harmonic current component.

<sup>2</sup>In the present implementation, the switch is only switched off during the initial transient of the power system.

<sup>3</sup>The implemented solution switches the current limiting loop off when the adaption of  $\underline{G}_f$  is finished. Using the current limiting controller to protect the circuit after startup has not been implemented.



The controller and adaption algorithm for one harmonic frequency is shown in Fig. 4.9. For each harmonic to be cancelled, one controller with its own reference frame has to be implemented. The outputs of all controllers as well as the output of the fundamental controller are summed since superposition applies in the stationary reference system.

The basic principle of the controller is the same as for the fundamental current control. The current is transformed to the rotating reference frame. With a linear phase low pass filter (*FIR* filter), the harmonic content of the specific frequency is extracted. The harmonic component is multiplied by  $\underline{G}_h$  to obtain the correct output voltage  $\underline{v}_{f,h}^e$  which produces the appropriate harmonic current.  $\underline{G}_h$  has to be adapted in such a way that the harmonic compensation current  $\underline{i}_{c,h}^e$  is equal to the harmonic load current  $\underline{i}_{r,h}^e$ .

The harmonic compensation current can be calculated as

$$\underline{i}_{c,h} = \frac{\underline{v}_{f,h}}{\underline{Z}_{fh}} \quad (4.18)$$

assuming that the source voltage is strong enough such that  $\underline{v}_{t,h} = 0$ . Ideally the compensation current  $\underline{i}_{c,h}$  should be equal to the load distortion current  $\underline{i}_{r,h}$ . According to the block diagrams in Fig. 3.11 and Fig. 4.9, the overall transfer function of one harmonic component can be described as

$$\underline{v}_{f,h} = \underline{H}_P \underline{H}_D \underline{G}_h \underline{H}_C \underline{H}_A \underline{H}_I \underline{i}_{r,h} \quad (4.19)$$

where  $\underline{G}_h$  is the transfer function of the *DSP* algorithm for the harmonic components. All of the transfer functions are assumed linear and change only the phase and magnitude of the sinusoidal signal, i. e.  $\underline{H} = \underline{H}(h\omega_s)$ . The only parameter that can be changed in (4.19) is  $\underline{G}_h$ . In the ideal case where the compensation current  $\underline{i}_{c,h}$  is equal to the harmonic load current  $\underline{i}_{r,h}$ ,  $\underline{G}_h$  results in

$$\underline{G}_h = \frac{\underline{Z}_{fh}}{\underline{H}_P \underline{H}_D \underline{H}_C \underline{H}_A \underline{H}_I} \quad (4.20)$$

The most dominant values in (4.20) are the filter impedance  $\underline{Z}_f$  and the delays  $\underline{H}_D$  and  $\underline{H}_P$ . Therefore, a good initial value for  $\underline{H}_h$  is

$$\underline{G}_{h0} = \frac{\underline{Z}_{fh}}{\underline{H}_P \underline{H}_D} = \underline{Z}_{fh} e^{j2h\omega_s T_T} \quad (4.21)$$

Since small phase errors in the compensation current result in much worse performance than small errors in magnitude, the phase and magnitude are adapted separately. Also, the fact that delays are mainly present in the system which result in phase shifts justifies this approach. The drawback of this method is that the currents  $\underline{i}_c^{he}$  and  $\underline{i}_r^{he}$  have to be converted from a rectangular to a polar coordinate system. This results in additional computational effort.<sup>4</sup> The magnitude and phase error are calculated as

$$\begin{aligned} I_e^{he} &= |\underline{i}_{c,h}^{he}| - |\underline{i}_{r,h}^{he}| \\ \varphi_e^{he} &= \angle \underline{i}_{c,h}^{he} - \angle \underline{i}_{r,h}^{he} \end{aligned} \quad (4.22)$$

The errors are integrated after multiplying with  $A_h$  which defines the adaption speed

$$\begin{aligned} G_{eh}[n] &= G_{eh0} + \sum_{k=n_0}^n A_{Ih} \, en_{ah}[k] \, (I_e^{he}[k] * f_{iir}[k]) \\ \varphi_{eh}[n] &= \varphi_{eh0} + \sum_{k=n_0}^n A_{\varphi h} \, en_{ah}[k] \, (\varphi_e^{he}[k] * f_{iir}[k]) \end{aligned} \quad (4.23)$$

where switch  $en_{ah} = \{0, 1\}$  allows the ability to turn on and off the adaption of  $G_{eh}$  and  $\varphi_{eh}$ . Finally,  $\underline{G}_h$  results in

$$\underline{G}_h = \underline{G}_{h0} \, G_{eh} e^{\varphi_{eh}} \quad (4.24)$$

#### 4.4. Reference Frame Generator

In order to generate the five reference frames  $K^e$ ,  $K^{-5e}$ ,  $K^{7e}$ ,  $K^{-11e}$ , and  $K^{13e}$  that are necessary to control the fundamental and four harmonic currents, a phase locked loop (*PLL*) is implemented (Fig. 4.10).

The *PLL* consists of three main parts, the phase discriminator (*PD*), the loop filter,  $f_{pl}[n]$ , and the voltage controlled oscillator (*VCO*) [25]. The source terminal voltage  $\underline{v}_t^s[n]$  is used as a reference signal for the *VCO*. Taking into account only the fundamental component, the voltage can be written as

$$\underline{v}_{t,1}^s[n] = \sqrt{2} \, V_{t,1} \, e^{j\theta_s[n]} \quad (4.25)$$

---

<sup>4</sup>Since errors in magnitude do not result in significant reduction of compensation performance, it could be analyzed if satisfying results can be obtained by only adapting the phase  $\varphi_{eh}$

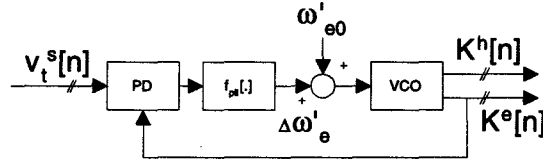


FIGURE 4.10: Phase-locked-loop with phase discriminator (*PD*) and voltage controlled oscillator (*VCO*).

$$\theta_s[n] = \theta_{s0} + \sum_{k=n_0}^n \omega'_s$$

where  $\omega'_s$  is the normalized frequency (normalized with the sampling frequency) corresponding to the source frequency  $f_s$ . The initial value for  $\theta_{s0}$  is the phase angle at startup of the control circuit. The reference frame rotating with fundamental frequency,  $\underline{K}^e$ , can be written in a similar way as

$$\begin{aligned} \underline{K}^e[n] &= e^{-j\theta_e[n]} \\ \theta_e[n] &= \theta_{e0} + \sum_{k=n_0}^n \omega'_e[k] \end{aligned} \quad (4.26)$$

where  $\omega'_e[n]$  is the normalized fundamental frequency used to generate the reference frame. This frequency has to be controlled in order to match the source frequency  $\omega_s$ . The phase discriminator transforms the reference voltage  $\underline{v}_t^s[n]$  to the rotating system using  $\underline{K}^e[n]$  and calculates the phase error  $\varphi_{err}[n]$

$$\varphi_{err}[n] = \angle \underline{v}_{t,1}^s[n] \underline{K}^e[n] = \theta_s[n] - \theta_e[n] = \theta_{s0} - \theta_{e0} + \sum_{k=n_0}^n (\omega'_s[k] - \omega'_e[k]) \quad (4.27)$$

In order to minimize the error at startup, the initial condition of the *VCO*,  $\theta_{e0}$ , is set to

$$\theta_{e0} = \theta_{s0} = \angle \underline{v}_{t,1}^s[n_0] \quad (4.28)$$

To reduce distortion due to harmonics in  $\underline{v}_{t,1}$  the phase error is filtered with the loop filter  $f_{pll}[\cdot]$ . The resulting frequency used to generate the reference frame is

$$\omega'_e[n] = \omega'_{e0} + \Delta\omega'_e[n] = \omega'_{e0} + \varphi_{err}[n] * f_{pll}[n] \quad (4.29)$$

## 4.5. Simulation

### 4.5.1. General

All the simulations for the active filter have been done in *SIMULINK* [11] using the *PLECS*-toolbox [12]. *SIMULINK* is a toolbox for *MATLAB* to simulate complex control systems. Unfortunately, it is rather difficult to simulate electrical circuits since it does not accept schematics or netlists. *PLECS* enhances *SIMULINK* with the capability to simulate electrical circuits directly by writing a netlist for the circuit. The electrical circuit consists of only ideal components. Elements such as resistors, inductors, and capacitors are approximated with a linear equation. Elements such as ideal diodes or ideal switches consist of two states, an on-state and an off-state. If they are in the on-state, the element is regarded as an ideal short circuit. If they are in the off-state, an open circuit is used for the simulation. The electrical circuit is simulated as a linear system between two switching states, i. e. the circuit is regarded as piece-wise linear. Therefore, this toolbox allows the ability to simulate a power electronic circuit and control circuits as a closed loop system within a short simulation time.

The drawback of using this tool is that component specific characteristics cannot be incorporated into the simulation, i. e. all nonlinear or parasitic characteristics are neglected in the simulation. The detailed simulation schematics and codes are given in Appendix C & D.

### 4.5.2. Startup of Power Circuit

One of the major difficulties of the active filter is the startup phase of the circuit and control algorithm. Due to arbitrary initial conditions of the circuit element states and control parameters, the initial transient can lead to high currents and voltage spikes which are harmful to the circuitry.

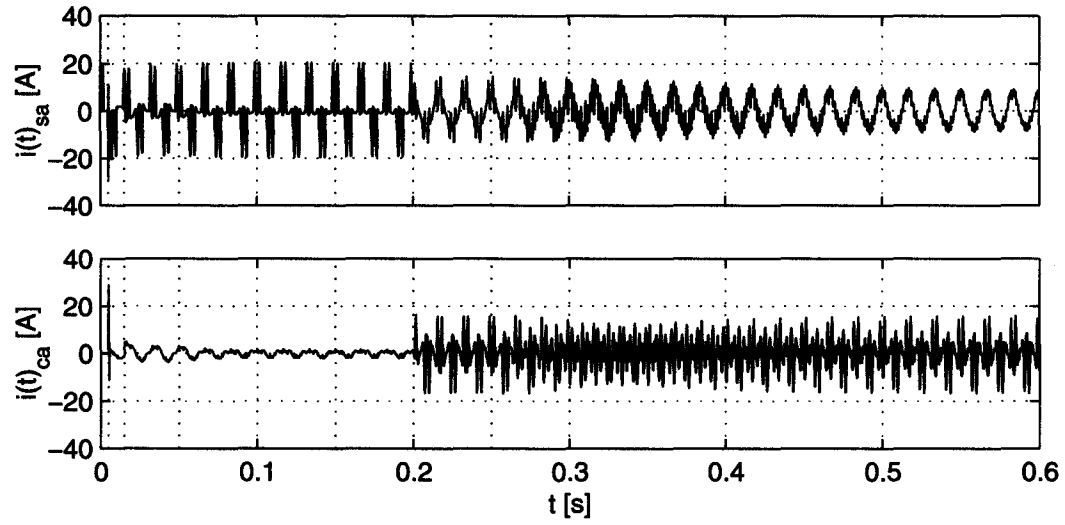


FIGURE 4.11: System currents at startup.

Fig. 4.11 shows the source current,  $i_{sa}$ , and compensation current,  $i_{ca}$ , during the startup phase of the power circuit and the active filter. The following phases are present:

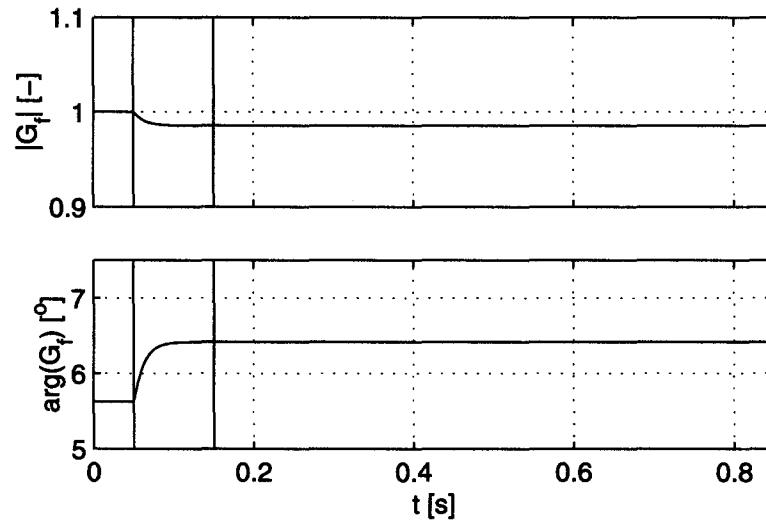


FIGURE 4.12: Adaption of fundamental correction factor.

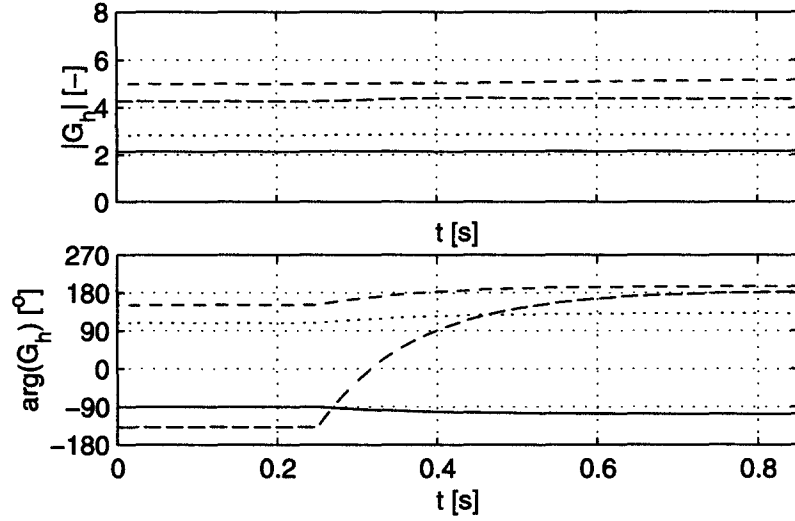


FIGURE 4.13: Adaption of harmonic correction factors.

**Power circuit:** ( $0 \leq t < 5ms$ ) Operate the power circuit without the active filter and switching ripple filter until the system is in steady state.

**Switching ripple filter:** ( $5ms \leq t < 15ms$ ) Operate the power circuit with switching ripple filter until the system is in steady state. Large current peaks are to be expected at turn on.

**Fundamental current limitation:** ( $15ms \leq t < 50ms$ ) Switch on the active filter with enabled fundamental current limiting loop to protect against high currents.

Parameter	Initial Value at $t = 0$	Final Value at $t = 850ms$
$\underline{G}_f$	$1.00 \angle 5.62^\circ$	$0.99 \angle 6.42^\circ$
$\underline{G}_5$	$2.13 \angle -90.17^\circ$	$2.15 \angle -106.85^\circ$
$\underline{G}_7$	$2.82 \angle 108.62^\circ$	$2.86 \angle 131.78^\circ$
$\underline{G}_{11}$	$4.27 \angle -138.317^\circ$	$4.37 \angle -177.55^\circ$
$\underline{G}_{13}$	$5.00 \angle 151.59^\circ$	$5.17 \angle -164.78^\circ$

TABLE 4.2: Initial and final values of adaption parameters.

The fundamental compensation current is high but within the limits of the system ratings. No adaption of  $\underline{G}_f$  is performed.

**Fundamental current adaption:** ( $50ms \leq t < 150ms$ ) With the adaption of  $\underline{G}_f$ , the fundamental compensation current is reduced to a small value. Fig. 4.12 shows the change of magnitude and phase of  $\underline{G}_f$  during the adaption process.

**Fixed fundamental current:** ( $150ms \leq t < 200ms$ ) The adaption of  $\underline{G}_f$  is turned off as well as the current limiting control loop.

**Harmonic current injection :** ( $200ms \leq t < 250ms$ ) Harmonic current is injected with the initial values for  $\underline{G}_h$  until all internal filters are in steady state.

**Harmonic current adaption :** ( $250ms \leq t < 850ms$ ) Adaption of  $\underline{G}_h$  to inject harmonic current with the correct phase and magnitude. In Fig. 4.11, it can be seen that for  $t \geq 500ms$  the resulting source current has only small harmonic distortion left. The adaption of  $\underline{G}_h$  for the four harmonic current components that are cancelled can be seen in Fig. 4.13.

As shown in Fig. 4.12 and Fig. 4.13, the adaption of the values  $\underline{G}_f$  and  $\underline{G}_h$  are mainly in phase rather than in magnitude. Tab. 4.2 summarizes the initial values and the final values of the adapted parameters at steady state of the simulation. The resulting small changes validate the assumptions made for the initial values  $\underline{G}_{f0}$  and  $\underline{G}_{h0}$ .

#### 4.5.3. Steady State Compensation

Once the adaption of  $\underline{G}_{f0}$  and  $\underline{G}_{h0}$  reaches a steady state situation, full harmonic compensation can be expected. Fig. 4.14 shows the source and compensation currents in the time and frequency domains. The signals in the time domain are filtered such that the current ripple due to the switching is eliminated and only the signals of interest are shown. As can be seen from the spectrum of the source current  $|I_{sa}(f)|$ , harmonic current components of lower harmonic orders  $h \leq 11$  are nearly eliminated. The spectrum of

k	$ I_{sa}(kf_s) [\text{A}]$	$ I_{ca}(kf_s) [\text{A}]$	$ I_{va}(kf_s) [\text{A}]$	$ I_{fa}(kf_s) [\text{A}]$	$ I_{ra}(kf_s) [\text{A}]$
1	6.18	0.16	1.38	1.33	6.33
5	0.03	5.13	0.00	5.13	5.14
7	0.03	4.11	0.00	4.11	4.12
11	0.08	1.91	0.00	1.91	1.91
13	0.01	0.97	0.00	0.97	0.98
$THD_{i\%}$	15.4 %				109.8 %

TABLE 4.3: Resulting system currents.

the compensation current,  $|I_{ca}(f)|$ , shows that the fundamental current component is reduced to a minimum. Since fundamental current is absorbed by the switching ripple filter current, the active filter has to compensate accordingly (Fig. 4.15). It also can be seen, that the switching ripple filter does not absorb any harmonic current components. The results are summarized in Tab. 4.3. Even though the harmonic source currents are low in magnitude, the  $THD_{i_s\%}$  is 15.4%. This results from two main causes. First,

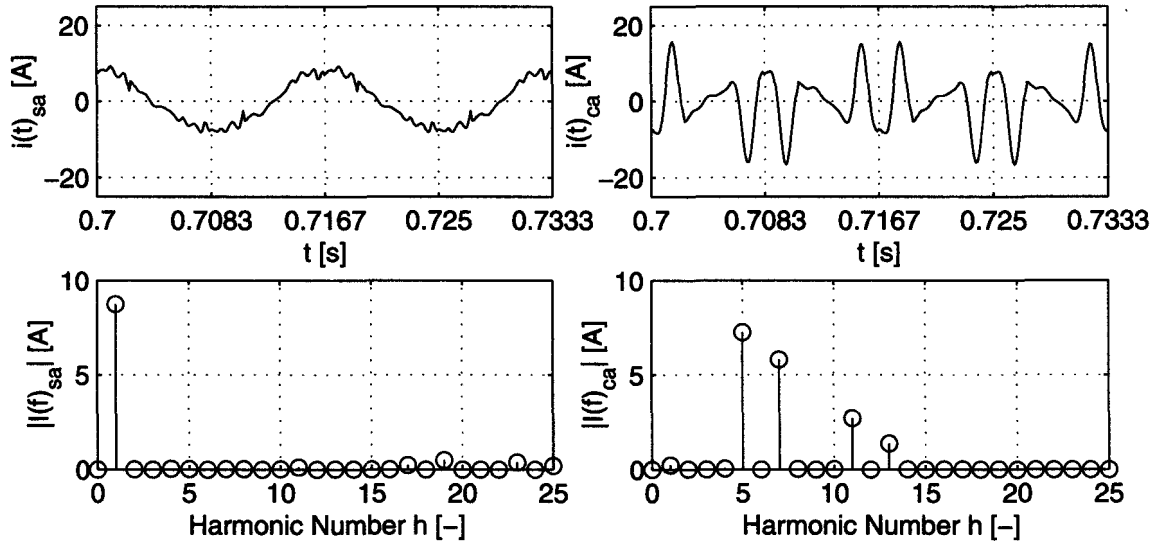


FIGURE 4.14: Source and compensation currents.



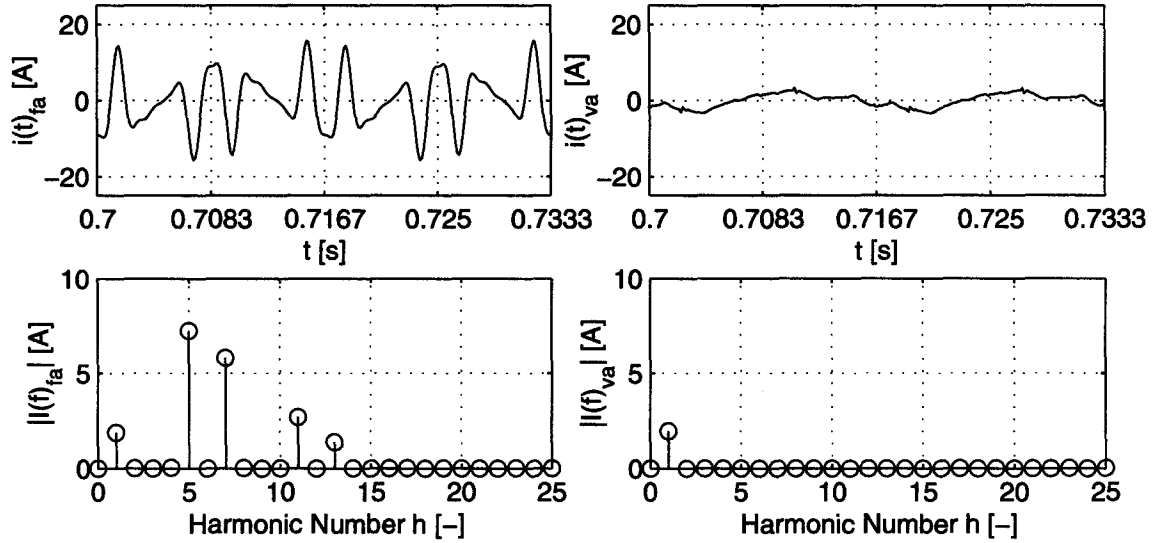


FIGURE 4.15: Active filter and switching ripple filter currents.

higher order harmonic currents are not cancelled, and second, high frequency distortion resulting from switching ripple current is present which is suppressed in the graphs of Fig. 4.14 and Fig. 4.15.

#### 4.5.4. Transient Behavior

The section above describes the startup of the active filter until it reaches steady state, and the cancellation results are shown as effective after  $t > 850ms$ . If an active filter is used in a system with frequent load changes, a filter also has to be able to react quickly to new distortion characteristics. As stated in (4.14) and (4.19), the input-output characteristic of the filter contains transfer functions that are only slowly varying with time, i. e. they can be regarded as constant. Once the correction factors  $\underline{G}_f$  and  $\underline{G}_h$  are determined for a particular set point, the system can quickly compensate for other set points, since no new adaption has to be performed. Of course, minor deviations from the optimal correction factors for the new set points can occur since the system is not entirely linear.

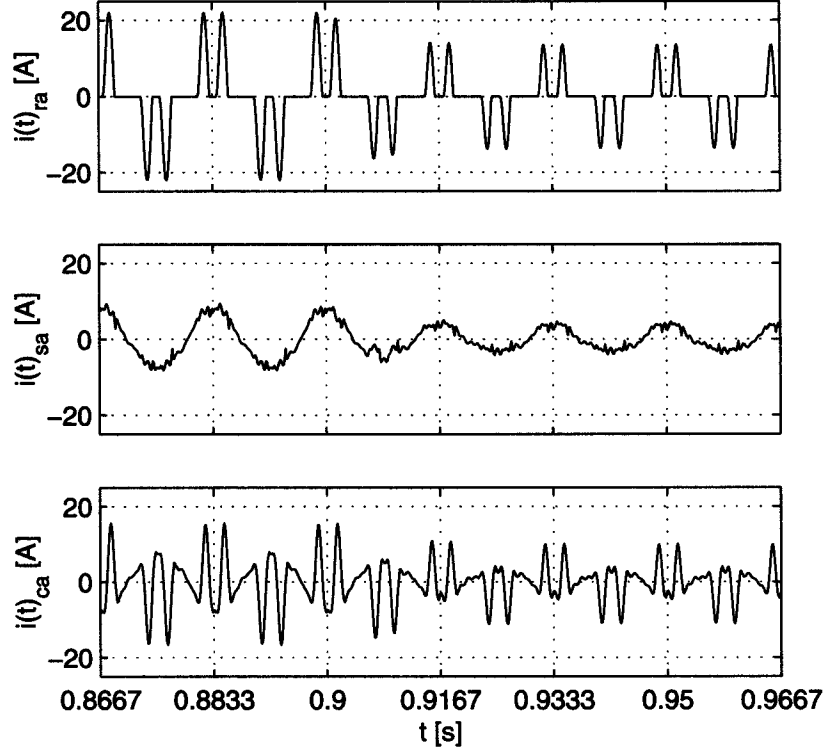


FIGURE 4.16: Currents during a load transient.

To simulate the validity of applying the parameters of one set point to another set point, the updating of the parameters is disabled ( $en_{ah} = 0$ ) for  $t > 850ms$  (refer to simulation in Fig. 4.11). At  $t = 900ms$ , the load is changed from  $R_L = 80\Omega$  to  $R_L = 160\Omega$  which results in a load power change from  $P_L \approx 5kW$  to  $P_L \approx 2.5kW$ . The load current transient as well as the change in source and compensation currents are shown in Fig. 4.16. The effectiveness of the filter on the new set point is shown in Fig. 4.17 and summarized in Tab. 4.4.

Characteristically the  $THD\%$  of the load current  $i_{ra}$  increases with reduced load since the double pulses are shorter in duration. On the other hand, the  $THD$  increase in the source power is mainly due to current ripple which is independent of the set point of the system.

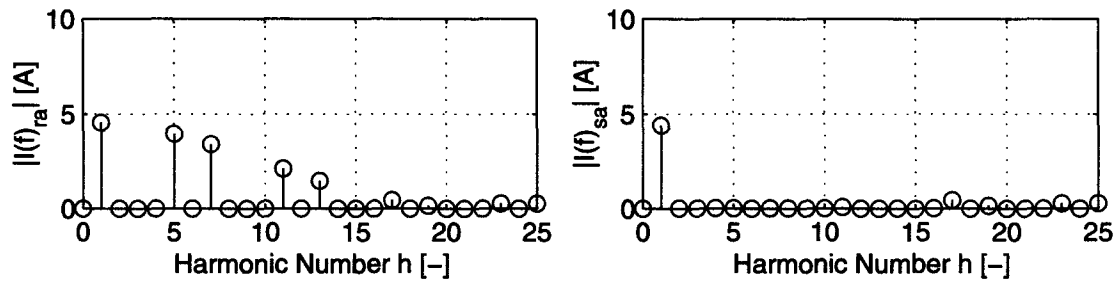


FIGURE 4.17: Current spectra after load transient.

k	$ I_{sa}(kf_s) $ [A]	$ I_{ca}(kf_s) $ [A]	$ I_{va}(kf_s) $ [A]	$ I_{fa}(kf_s) $ [A]	$ I_{ra}(kf_s) $ [A]
1	3.11	0.11	1.38	1.36	3.22
5	0.02	2.78	0.00	2.78	2.80
7	0.01	2.41	0.00	2.41	2.41
11	0.06	1.50	0.00	1.49	1.50
13	0.00	1.04	0.00	1.04	1.04
$THD_i\%$	29.0 %				128.8 %

TABLE 4.4: Resulting system currents after load transient.

#### 4.5.5. Switching Ripple Filter

Fig. 4.18 shows one period of high sampled current signals that show the extent of the high frequency current distortion resulting from the switching characteristic of the voltage source inverter. It can be seen that the filter current,  $i_{fa}$ , is highly distorted with current spikes as high as 10A. On the other hand, most of the ripple is absorbed by the switching ripple filter and results in a low distorted source current  $i_{sa}$ .

The large scale spectra of the currents  $i_{fa}$ ,  $i_{ca}$ , and  $i_{sa}$  are shown in Fig. 4.19. The spectra show that the switching ripple results in distortion with center frequencies of  $mf_T = m7680\text{Hz}$  with  $m = 1, 2, 3 \dots$

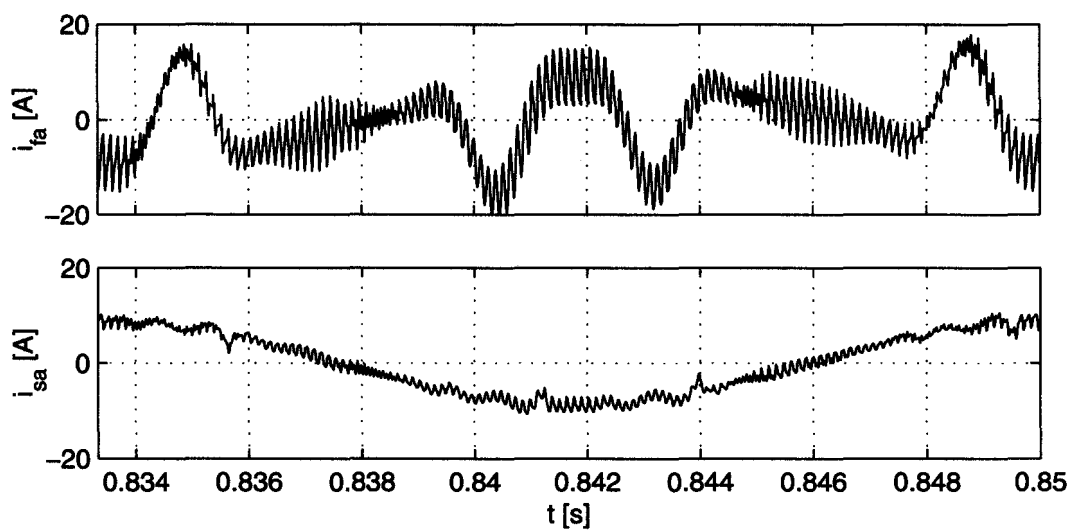


FIGURE 4.18: Unfiltered compensation and source current.

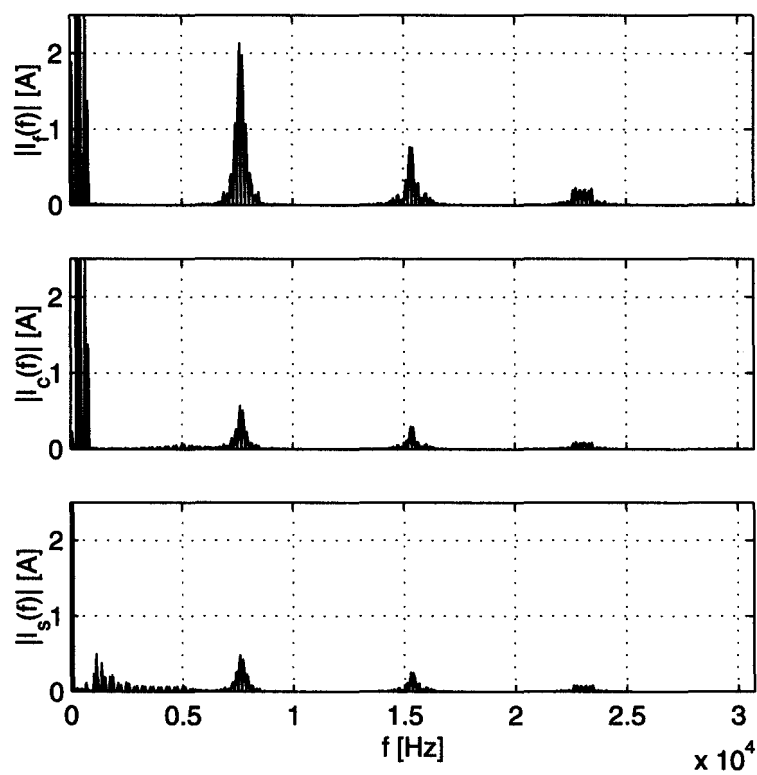


FIGURE 4.19: Wideband spectra of active filter, compensation, and source current.

## 5. SUMMARY OF RESULTS

### 5.1. Discussion

A three-phase active filter to cancel lower order harmonics has been proposed. During the research, numerous problems and solutions were encountered that can give ideas and motivation for future projects. Also, the results that were gained with the simulation of the system are satisfying and worthwhile to summarize.

A thorough investigation of a hardware implementation of the proposed algorithm has been performed. Unfortunately, a hardware implementation of the control algorithm is beyond the scope of a Master thesis.

The problems of the implementation arise mainly from two sides. On one side, the hardware circuit for the high power voltage source inverter imposes burdens. To design and build a stable gating circuit including power supply and electrical isolation requires experience and detailed knowledge of such circuits. The implementation of the hardware for another active filter has shown that extensive tuning of the circuit is necessary. On the other hand, an implementation of the active filter on the fixed-point *DSP* requires additional time. Even though the *DSP* implements all *IO*-ports that are necessary to build an active filter, the processor architecture of the target system turned out to be non-transparent. Numerous exceptions and restrictions in the command set and memory usage had to be taken into account and led to mistakes in implementation. In addition, the implementation in a fixed-point environment of the algorithm required exact knowledge of the number range for each calculation step in order to scale intermediate results and operations appropriately. Both the non-transparent architecture and the fixed-point number format would increase the time of software implementation even though this was not a focus of the research. It is suggested that for future research, a floating-point processor architecture be used that can be programmed in a high-level language. This would greatly reduce the implementation time since the

same code structure could be used as for simulation and no transformation to a fix-point environment is necessary.

The proposed algorithm is based on rotating reference frames for each harmonic component that has to be cancelled. In contrast to the widely used  $pq$ -based active filters, the proposed approach allows for the extraction and control of each harmonic component separately. In the case of hardware limitations such as current rating, the cancellation can be controlled to be maximized within limits of the system. Also, the proposed algorithm can be extended with a cost-function defining harmonic current cancellation and power factor correction performance which could then be maximized.

## 5.2. Conclusions

Solid-state power electronic devices provide efficient transformation of electric power. Unfortunately, those devices used in a power system generate unwanted voltage and current distortion due to their nonlinear characteristics. With the increase in use of power electronic converters from wall-powered consumer electronic devices to high power inverters, the pollution on power distribution systems will increase and solutions to eliminate the pollution are required. This project focuses on the reduction of low order harmonic current distortion.

The thesis describes one possible implementation of a shunt active power filter. The proposed approach employs the use of a three-phase inverter bridge consisting of six *IGBTs* and a *dc*-voltage source. The inverter is connected in parallel with the power system over coupling inductors. The control strategy is based on synchronous rotating reference frames to filter harmonic components and cancel them accordingly. The simulation results show that after a startup phase, the active filter nearly eliminates 5<sup>th</sup>, 7<sup>th</sup>, 11<sup>th</sup>, and 13<sup>th</sup> harmonic components in the source current. It is also shown that the proposed control strategy can react quickly to load changes and achieves very good cancellation results, even with old parameters.

Unfortunately, after a thorough investigation it has been concluded that an implementation of the active filter on the fixed point *DSP* is beyond the scope of a Master's research project. Because of this reason, the hardware implementation is not realized and therefore no experimental verification of the proposed filter strategy is available.

### 5.3. Future Recommendation

The active power filter control strategy presented in this thesis is designed to cancel lower order harmonics on three-phase, balanced power distribution systems. The design can be extended to not only cancel higher order harmonics but also to reduce harmonics in three-phase, four-wire unbalanced systems.

The inverter used for the active filter is implemented with a *dc*-voltage source. In order to reduce hardware, the system should be extended to use a *dc*-capacitor that is charged from the power line as originally shown in Fig. 3.6. In order to maintain a constant *dc*-voltage, real power has to be absorbed in a controlled manner from the power line to compensate for losses in the inverter.

The active power filter studied in this thesis is applied on the low voltage side of an industrial power system. To economically justify the use of an active filter, the filter might have to be redesigned to reduce harmonics on the high voltage side, i. e. at the point of common coupling (*PCC*) (Fig. 1.1). In order to do so, the switching frequency of  $f_T = 7680Hz$  might have to be reduced to a frequency of  $< 2000Hz$ . The use of a neutral point clamped (*NPC*) inverter could be studied to increase the ratings of the inverter and to reduce switching ripple.

Of course, in order to gain experimental results, a complete prototype implementing the active filter should be built. The experimental results should not only be used to verify the simulation but moreover the differences between simulation and experimental results should be studied intensively in order build good models for future projects. This would reduce the development time since more problems could then be discovered during the simulation process.

## BIBLIOGRAPHY

1. Roger C. Dugan, Mark F. McGranaghan, and H. Wayne Beaty, *Electrical power systems quality*, McGraw-Hill, 1996.
2. IEEE Working Group on Power Systems, "Recommended practice for monitoring electric power quality," *IEEE Standard 1159-1995*, 1995.
3. Anette von Jouanne, *New Passive And Active Filtering Techniques for The Mitigation of Power System Harmonics and to Reduce the effects of High Frequency PWM Switching on the Operation of AC Motor Drive*, Ph.D. thesis, Texas A&M University, 1995.
4. IEEE Working Group on Power Systems, "Electrical power systems quality," *IEEE Transactions on Power Apparatus and Systems*, vol. PAS-102, pp. 2455-2460, August 1983.
5. W. Mack Grady, Marek J. Samotyj, and Antonio H. Noyola, "Survey of active power line conditioning methodologies," *IEEE Transactions on Power Delivery*, vol. 5, no. 3, pp. 1536-1542, July 1990.
6. Working Group on Monitoring Electrical Power Quality of SCC22, "Recommended practice on monitoring electric power quality," *IEEE P1159*, vol. PAS-102, November 1992.
7. Hirofumi Akagi, "Trends in active power line conditioners," *IEEE Transactions on Power Electronics*, vol. 9, no. 3, May 1994.
8. Hirofumi Akagi, Yukifumi Tsukamoto, and Akira Nabae, "Analysis and design of an active power filter using quad-series voltage source pwm converters," *IEEE Transactions on Industry Applications*, vol. 26, no. 1, pp. 93-98, January-February 1990.
9. Bhim Singh, Kamal Al-Haddad, and Ambrish Chandra, "Review of active filters for power quality improvement," *IEEE Transactions on Industrial Electronics*, vol. 46, no. 5, pp. 960-971, 1999.
10. Fang Z Peng and Donald J. Adams, "Harmonic sources and filtering approaches," *Conference Record - IAS Annual Meeting (IEEE Industry Applications Society)*, pp. 448-455, October 1999.
11. The MathWorks, Inc., *MATLAB*, October 1999.
12. J.H. Allmeling and W.P. Hammer, "Plecs - piece-wise linear electrical circuit simulation for simulink," *Proceedings of the IEEE International Conference on Power Electronics and Drive Systems*, vol. 1, pp. 355-360, 1999.



13. Abdurrahman Unsal, *DSP controlled Resonant active power filter for low-order current harmonic compensation*, Ph.D. thesis, Oregon State University, 2000.
14. Paul C. Krause, Oleg Wasynczuk, and Scott D. Sudhoff, *Analysis of Electric Machinery*, IEEE Press, 1994.
15. Hirofumi Akagi, Y. Kanazawa, and A. Nabae, "Instantaneous reactive power compensators comprising switching devices without energy storage components," *IEEE Transactions on Industry Applications*, vol. IA20, no. 3, pp. 625–630, May/June 1984.
16. S. Bhattacharya and D. Divan, "Synchronous frame based controller implementation for a hybrid series active filter system," *IEEE Conference on Industry Applications*, pp. 2531–2540, 1995.
17. H. Akagi and A. Nabae, "p-q theory in three-phase systems under non-sinusoidal conditions," *European Transactions on Electrical Power Engineering*, vol. 3, no. 1, pp. 27–31, January-February 1993.
18. Hirofumi Akagi, Satoshi Ogasawara, and Hyosung Kim, "Theory of instantaneous power in the three-phase four-wire systems: a comprehensive approach," *Conference Record - IAS Annual Meeting (IEEE Industry Applications Society)*, pp. 431–439, Oct 1999.
19. Heinz Willi van der Broeck, Hans-Christoph Skudeliny, and Georg Viktor Stanke, "Analysis and realizaton of a pulsesidth modulator based on voltage space vectors," *IEEE Transactions on Industrial Application*, vol. 24, no. 1, January 1988.
20. Texas Instruments, *TMS320C24x DSP Controllers, Peripheral Library and Specific Devices*, 1998.
21. Arun K. Guru, Juan Carlos Balda, Ken Carr, and Y.Q. Xiang, "Design of a switching-ripple filter for a shunt-connected active power filter," *Conference Record - IAS Annual Meeting (IEEE Industry Applications Society)*, pp. 1364–1368, October 1998.
22. Sami Valiviita and Seppo J. Ovaska, "Delayless method to generate current reference for active filters," *IEEE Transaction on Industrial Electronics*, vol. 45, no. 4, pp. 559–567, August 1998.
23. Seung-Gi Jeong and Myung-Ho Woo, "Dsp-based active power filter with predictive current control," *IEEE Transactions on Industrial Electronics*, vol. 44, no. 3, pp. 329–336, January 1997.
24. Vasco Soares, Pedro Verdelho, and Gil D. Marques, "An instantaneous active and reactive current component methode for active filters," *IEEE Transaction on Power Electronics*, vol. 15, no. 4, pp. 660–669, July 2000.

25. Vikram Kaura and Vladimir Blasko, "Operation of a phase locked loop system under distorted utility conditions," *IEEE Transactions on Industry Applications*, vol. 33, no. 1, pp. 58–63, Januar-February 1997.
26. Oregon State University Graduate School, *Preparing a Thesis or Dissertation at Oregon State University: A Graduate Student's Guide*, September 1995.
27. Ned Mohan, Tore M. Undeland, and William P. Robbins, *Power Electronics: converters, applications, and design*, John Wiley & Sons, Inc., 2nd edition, 1995.
28. Benjamin C. Kuo, *Automatic Control Systems*, Prentice Hall, 7nd edition, 1995.
29. Gene F. Franklin, J. David Powel, and Michael L. Workman, *Digital Control of Dynamic Systems*, Addison-Wesley Publishing Company, 2nd edition, 1990.
30. Yukihiro Sato, Shin Nagayama, Hidenori Chigira, and Teruo Kataoka, "Adaptive control strategy for active power filters with voltage detection," *Conference Record - IAS Annual Meeting (IEEE Industry Applications Society)*, pp. 1356–1363, October 1998.
31. A.R. Bakhshai, G. Joos, and P. Jain, "Novel single pulse and pwm var compensator for high power applications," *Conference Record - IAS Annual Meeting (IEEE Industry Applications Society)*, pp. 1385–1392, October 1998.
32. S. Bhattacharya, T. M. Frank, D. M. Divan, and B. Banerjee, "Active filter system implementation," *IEEE Industry Application Magazine*, September-October 1998.
33. W. le Roux and J. D. van Wyk, "Modeling of distortion compensation ineffectivity in filters for non-active power," *IEEE Transactions on Industrial Electronics*.
34. L. Malesani and P. Mattavelli, "Robust dead-beat current control for pwm rectifiers and active filters," *Conference Record - IAS Annual Meeting (IEEE Industry Applications Society)*, pp. 1377–1384, October 1998.
35. Vladimir Blasko, "Adaptive filtering for selective elimination of higher harmonics from line currents of a voltage source converter," *Conference Record - IAS Annual Meeting (IEEE Industry Applications Society)*, pp. 1222–1228, October 1998.
36. Keiju Matsui, Tadashi Yamaguchi, Kazuo Tsuboi, and Fukashi Ueda, "Simple harmonic meter using phase locked loop," *IECON Proceedings (Industrial Electronics Conference)*, pp. 1550–1553, 1998.
37. Fang Zheng Peng, "Application issues of active power filters," *IEE Industry Application Magazine*, September-October 1998.
38. Gerard Leonardus van Harmelen and Johan H. R. Enslin, "Real-time dynamic control of dynamic power filters in supplies with high contamination," *IEEE Transactions on Power Electronics*, vol. 8, no. 3, pp. 301–308, July 1993.

39. Andrea Cavallini and Gian Carlo Montanari, "Compensation strategies for shunt active-filter control," *IEEE Transactions on Power Electronics*, vol. 9, no. 6, pp. 587–593, November 1994.
40. Hirofumi Akagi, Yukifumi Tsukamoto, and Akira Nabae, "Instantaneous reactive power compensators comprising switching devices without energy storage components," *IEEE Transactions on Industry Applications*, vol. 20, no. 3, May-June 1984.

## APPENDICES

## A GRAPH CREATION AND SPECTRA CALCULATION

All the graphs in this document are created from simulation data derived either in *MATLAB* or in *SIMULINK*.

All the graphs in the time domain except Fig. 4.18 are created from data sampled with  $f_s = 7680Hz$ . The highest frequency components in those signals are well beyond Nyquist rate of  $\frac{f_s}{2} = 3840Hz$  which would technically violate the sampling theorem. But since the graphs are only used for demonstration, the filtering effect of the low sampling frequency has positive effect. Since the sampling frequency is low, data of the whole simulation could be stored without exceeding memory limits.

The graph in Fig. 4.18 shows higher frequency components than just  $\frac{f_s}{2} = 3840Hz$ . In order to do so, the simulation signal is 32 times oversampled resulting in a sampling frequency of  $245.760kHz$ . With this high sampling frequency, the switching ripple is visible unlike in the figure created as described above. Because of the high sampling frequency, only data for the last fundamental period could be stored to not exceed the memory limits.

For the spectra and the calculations of the harmonic current components, the same oversampled vectors are used. In order to acquire valid results, the last period of the simulation when in steady state is used and the Fast Fourier Transformation (*FFT*) in *MATLAB* is applied. The spectra have a resolution of  $60Hz$  from  $0Hz$  to  $122.880kHz$ . The spectra show the peak values of the harmonic components, i. e. a division by  $\sqrt{2}$  is necessary to obtain the *rms*-values of the harmonic components.

## B NOMENCLATURE

Symbol	Unit	Description
<i>Variable representation</i>		
$f = f(t)$		regular real variable
$\mathbf{f} = \mathbf{f}(t)$		vector or matrix
$\underline{f} = \underline{f}(t)$		complex number
$F$		<i>rms</i> -value if $f(t)$ is an <i>ac</i> -signal, <i>dc</i> -value if $f(t)$ is an <i>dc</i> -signal
$F(f)$		spectrum of $f(t)$ when in steady state
<i>Variable transformation</i>		
$\mathbf{f}$		variable in three-phase system $\mathbf{f} = [f_a \ f_b \ f_c]^T$
$\mathbf{f}^s$		$\mathbf{f}$ transformed to stationary reference frame, vector notation, $\mathbf{f}^s = [f_d^s \ f_q^s]^T$
$\underline{f}^s$		$\mathbf{f}$ transformed to stationary reference, complex notation, $\underline{f}^s = f_d^s + j f_q^s$
$\mathbf{f}^e$		$\mathbf{f}$ transformed to reference frame rotating synchronous with frequency $\omega_e$ , vector notation, $\mathbf{f}^e = [f_d^e \ f_q^e]^T$
$\underline{f}^e$		$\mathbf{f}$ transformed to reference frame rotating synchronous with frequency $\omega_e$ , complex notation, $\underline{f}^e = f_d^e + j f_q^e$
$\mathbf{K}^s$		transformation matrix from three-phase variables to stationary, two-phase reference frame
$\mathbf{K}'^s$		transformation matrix from stationary, two-phase reference frame to three-phase variables
$\mathbf{K}^e$		transformation matrix to rotating reference frame synchronous to $\omega_e$ , vector-matrix notation
$\underline{K}^e$		transformation variable to rotating reference frame synchronous to $\omega_e$ , complex notation

Symbol	Unit	Description
<i>Signals and circuit elements</i>		
$\mathbf{v}_s$	[V]	source voltage
$\mathbf{v}_t$	[V]	source terminal voltage
$\mathbf{v}_f$	[V]	active filter terminal voltage
$v_{rd}$	[V]	<i>dc</i> -bus voltage of rectifier load
$v_{fd}$	[V]	<i>dc</i> -bus voltage of active filter
$\mathbf{i}_s$	[A]	source current
$\mathbf{i}_r$	[A]	load current
$\mathbf{i}_c$	[A]	compensation current
$\mathbf{i}_f$	[A]	active filter current
$\mathbf{i}_v$	[A]	switching ripple filter current
$i_{rd}$	[A]	rectifier load <i>dc</i> -bus current
$i_L$	[A]	<i>dc</i> -load current
$i_{fd}$	[A]	active filter <i>dc</i> -bus current
$R_s$	[Ω]	source resistance
$L_s$	[H]	source inductance
$R_c$	[Ω]	cable resistance
$L_c$	[H]	cable inductance
$R_f$	[Ω]	coupling inductor losses
$L_f$	[H]	coupling inductor
$R_v$	[Ω]	switching ripple filter resistor
$L_v$	[H]	switching ripple filter inductor
$C_v$	[F]	switching ripple filter capacitor
$R_{rd}$	[Ω]	<i>dc</i> -link inductor losses
$L_{rd}$	[H]	<i>dc</i> -link inductor
$C_{rd}$	[F]	<i>dc</i> -bus capacitor
$R_L$	[Ω]	load resistor
$L_L$	[H]	load inductor

Symbol	Unit	Description
<i>Transfer functions</i>		
$\underline{H}_C$	[-]	current transducer
$\underline{H}_V$	[-]	voltage transducer
$\underline{H}_A$	[-]	anti-aliasing filter
$\underline{H}_C$	[-]	analog-digital converter
$\underline{H}_D$	[-]	calculation delay
$\underline{H}_P$	[-]	<i>PWM</i> circuit
$\underline{G}_f$	[-]	fundamental correction variable
$\underline{G}_h$	[-]	harmonic correction variable
$f_{fir}$	[-]	<i>FIR</i> -filter for harmonic extraction
$f_{iir}$	[-]	<i>IIR</i> -filter for adaption algorithm filtering
$f_{pll}$	[-]	<i>PLL</i> loop-filter
<i>Various variables</i>		
$f_s$	[Hz]	fundamental source frequency ( $f_s = 60Hz$ )
$f_T$	[Hz]	sampling frequency ( $f_T = 128f_s = 7680Hz$ )
$f_p$	[Hz]	switching frequency of <i>PWM</i> ( $f_p = f_T = 128f_s = 7680Hz$ )
$T_T$	[s]	sampling period ( $T_T = \frac{1}{f_t}$ )
$t_d$	[s]	delay time
$\varphi_d$	[°]	delay angle
$en_f$	[-]	enable fundamental injection
$en_h$	[-]	enable harmonic injection
$en_{if}$	[-]	enable current limiting loop
$en_{af}$	[-]	enable fundamental adaption
$en_{ah}$	[-]	enable harmonic adaption



## C COMPLETE SIMULATION CIRCUIT DIAGRAM

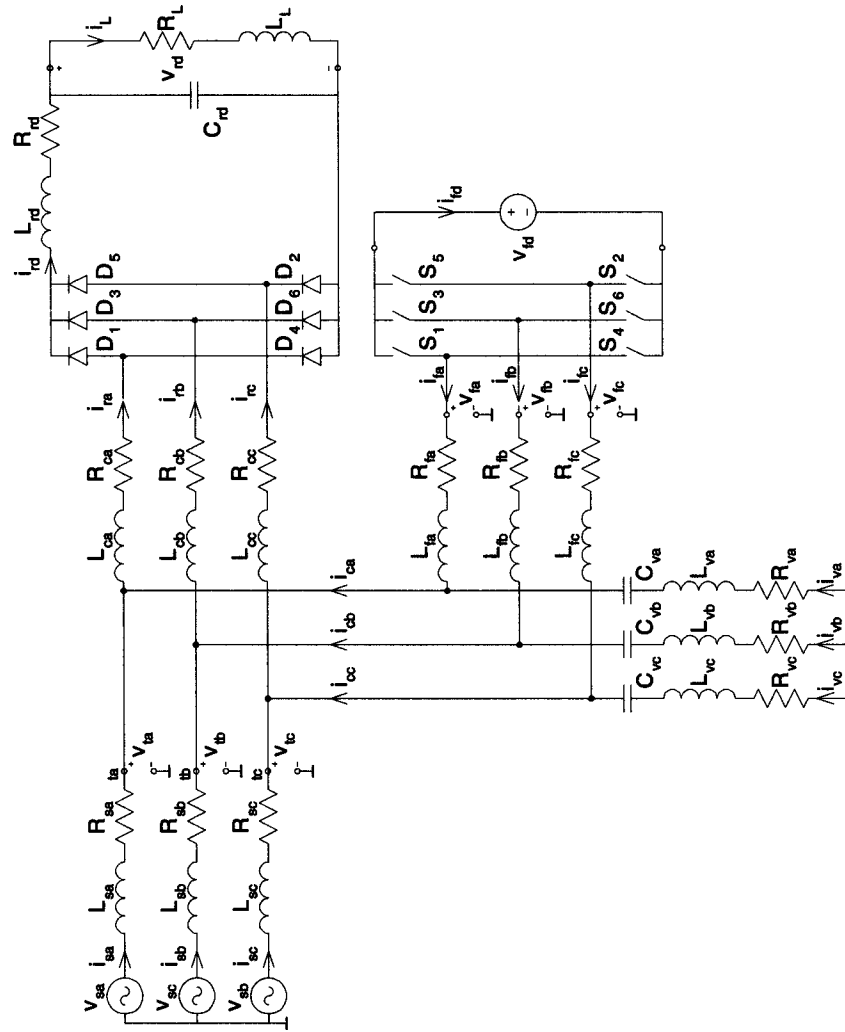


FIGURE C.1: Complete simulation circuit diagram.

## D SIMULATION FILES

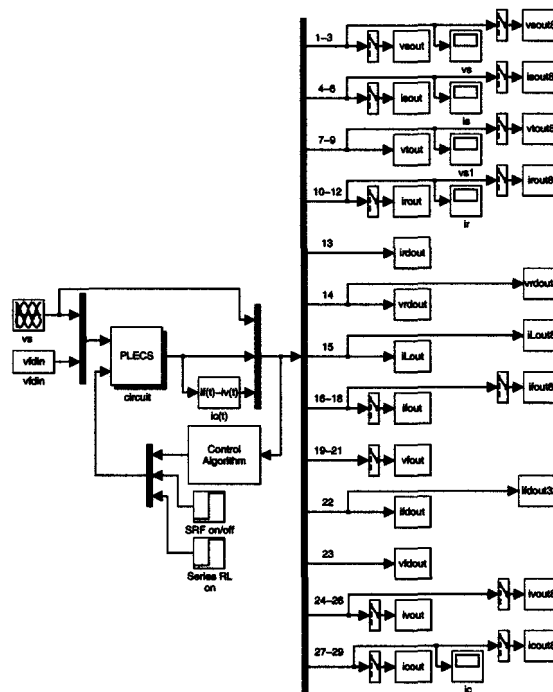


FIGURE D.1: *SIMULINK* model: Top level with *PLECS* circuit interface and data recording.

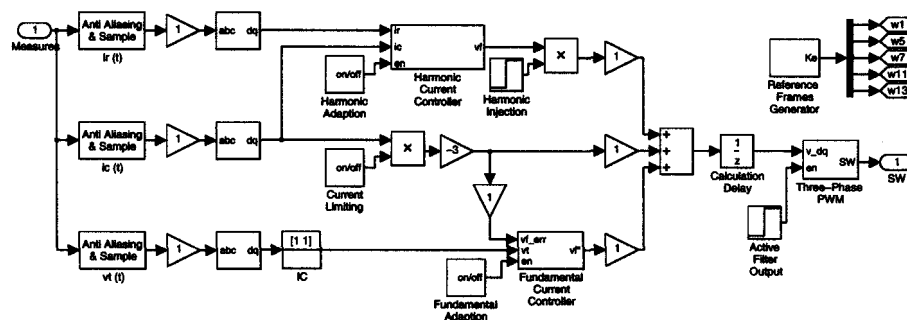


FIGURE D.2: *SIMULINK* model: Control algorithm.

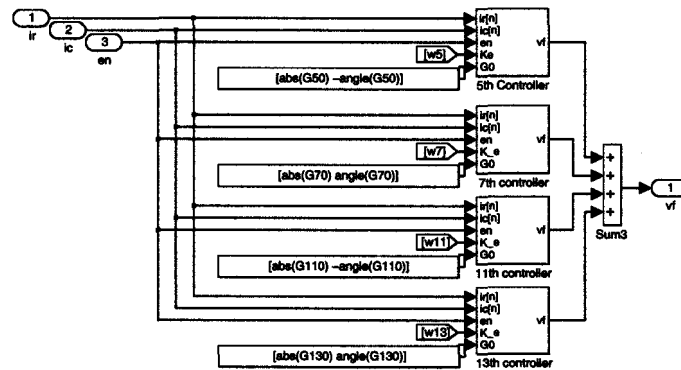


FIGURE D.3: *SIMULINK* model: All harmonic current controllers.

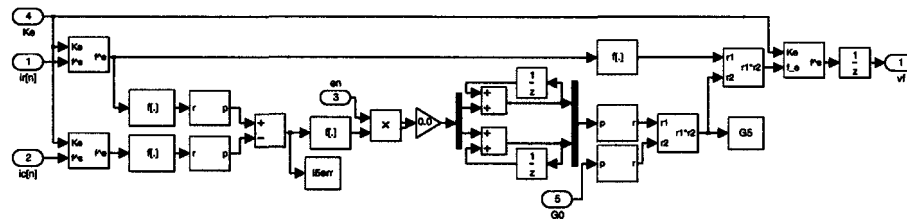


FIGURE D.4: *SIMULINK* model: Harmonic current controller for 5th harmonic.

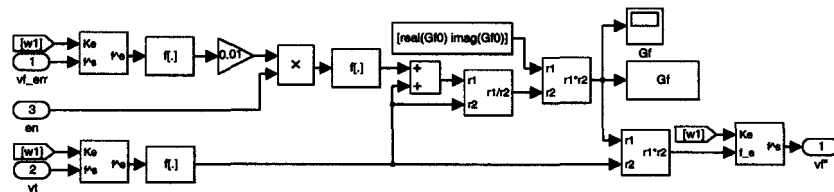


FIGURE D.5: *SIMULINK* model: Fundamental current controller.

```

%INIT initializes the SIMULINK simulation [OSU,MS]
%-----
%
% Author      : Marcel Merk
% Date       : 02/20/2000
%
% Add. Files  : circuit.tpx
%               circuit.m
%
% FILE DESCRIPTION
%   Initializes parameters and files that are used in the other simulation
%   files in this directory
%
% IMPORTANT NOTE
%   start first with init on the MATLAB command line
%
% INPUT PARAMETERS
%   none
%
% Developing System : IBM-PC
% Tool              : Matlab, Version 5.2.0
%
% Starting Date    : 02/20/2000
% Update          : 08/25/2000
%
%-----
% initialize general parameters -----
fs      = 60;                % source voltage frequency
nos     = 128;               % number of samples per periode
fT      = fs/nos;            % sampling frequency
TT      = 1/fT;              % sample time
mmor    = inf;               % maximum rows of samples to WS

% create PLECS file with parameters above -----
circuit;                     % init. circuit parameters
plecsrep ('circuit.tpx','circuit.tpl'); % substitute var. with values (.tpl)
plecs circuit;               % create PLECS system (.pld)

% define normalizing factors -----
Inorm = 20;
Vtnorm = 450;
Vfdnorm = vfdin;

% define switch on and off times -----
tsrf_on = 0.005;             % switch ripple filter on
tsrf_off = 0.015;            % active filter on
til_on = 0.015;              % current loop on
til_off = 0.15;              % current loop off
tvl_on = 0.05;               % fundamental voltage ctrl. on
tvl_off = 0.15;              % fundamental voltage ctrl. off
thc_on = 0.2;                % harmonic cancelation on
tha_on = 0.25;               % harmonic addaption on
tha_off = 0.85;              % harmonic addaption off

% design LP filter for extraction -----
b_fir = firls(63,[0 1 240 7680/2]/7680*2,[1 1 0 0],[100 1]);
a_fir = [1];

```

```

b_iir = [0.5821 1.1642 0.5821]*1e-3;
a_iir = [1.0000 -1.9306 0.9329];

b_vctr = b_iir;              % filter for vf_1 control
a_vctr = a_iir;

b_hctr = b_iir;              % filter for harmonic phase ctrl
a_hctr = a_iir;

b_hfil = b_fir;              % filter for harmonic extraction
a_hfil = a_fir;

Kv      = 100/(2*pi*6);
a       = exp(-TT*2*pi*6);
b_pll   = [Kv];               % works better
a_pll   = [1 -a];             % works better

% design butterworth filter (anti aliasing filter) -----
if 1,
    Rpfilt = 3;
    Rsfilt = 40;
    Wp      = 19*60*2*pi;
    Ws      = 7680/2*2*pi;
    % [N,Wn] = buttord(Wp,Ws,Rp,Rs,'s');
    % [ba,aa] = butter(N,Wn,'s');

    % [ba,aa] = butter(2,2*pi*7680/3,'s'); %papis definition
    % [b_ct,a_ct] = butter(2,2*pi*7680/3,'s'); %papis definition
    % [b_vt,a_vt] = butter(2,2*pi*7680/3,'s'); %papis definition
    % [ba,aa] = butter(2,2*pi*2000,'s'); %low wp
end;

% initial condition for correction coefficients -----
jw      = j*2*pi*60;          % fundamental
H_PWN   = exp(-jw*TT);
H_DELE  = exp(-jw*TT);
Gf0     = 1/(H_PWN*H_DELE);

jw      = j*2*pi*5*60;        % 5th harmonic
Zf      = Rf + jw*Lf;
H_PWN   = exp(-jw*TT);
H_DELE  = exp(-jw*TT);
G50     = Zf/(H_PWN*H_DELE);

jw      = j*2*pi*7*60;        % 7th harmonic
Zf      = Rf + jw*Lf;
H_PWN   = exp(-jw*TT);
H_DELE  = exp(-jw*TT);
G70     = Zf/(H_PWN*H_DELE);

jw      = j*2*pi*11*60;       % 11th harmonic
Zf      = Rf + jw*Lf;
H_PWN   = exp(-jw*TT);
H_DELE  = exp(-jw*TT);
G110    = Zf/(H_PWN*H_DELE);

jw      = j*2*pi*13*60;       % 13th harmonic
Zf      = Rf + jw*Lf;
H_PWN   = exp(-jw*TT);
H_DELE  = exp(-jw*TT);

```

```
G130 = Zf/(H_PWM*H_DEL);
% end of init -----
```

```
%CIRCUIT simulation circuit parameter for PLECS circuit [OSU,MS]
```

```

%-----
%
% Author      : Marcel Merk
% Date       : 02/20/2000
%
% Add. Files  : circuit.tpx
%
% FILE DESCRIPTION
% Sets circuit parameters
%
% IMPORTANT NOTE
% is called by init
%
% INPUT PARAMETERS
% none
%
% Developing System : IBM-PC
% Tool              : Matlab, Version 5.2.0
%
% Starting Date    : 02/20/2000
% Update          : -
%
%-----

```

```

% initialize circuit parameters -----
SW = 1; % activate AF
measures= 29; % number of measurements

vs_ll = 460; % source voltage line to line

Ls = 44.9e-6; % source inductanceXXX
%Ls = 100e-6; % source inductance
Rs = 4.23e-3; % source resistance
Lc = 118e-6; % cable inductance
Rc = 0.5; %1.969; % cable resistance

Lrd = 1e-6; % rect. smooth inductor
Rrd = 0.1; % rect. resistance of smooth L
Crd = 2.5e-3; % rect. dc-capacitor
vcrd0 = 627; % initial value of Crd

RL = 80; % load resistor
LL = 1e-6; %1e-6 % load inductor

%Rv = 0.2/1.5; % SRF resistance
%Cv = 3.45e-6*1.5; % SRF capacitance
%Lv = 124e-6/1.5; % SRF capacitance

Rw = 1; % SRF resistance
Cw = 20e-6; % SRF capacitance
Rv = 0.5; % SRF resistance
Lv = 31.08e-6; % SRF capacitance

```

```

Cv = 13.82e-6; % SRF capacitance
Rf = 1; % active filter resistance
Lf = 1e-3; % active filter inductance
vfdin = 800/2; % active filter voltage source

%Lf = 5e-3; % active filter inductance
%vfdin = 1000/2; % active filter voltage source

```

```
% end of circuit.m -----
```

```
%circuit.tpx PLECS netlist for circuit simulation[OSU,MS]
```

```

$-----
$
$ Author      : Marcel Merk
$ Date       : 07/20/2000
$
$ Add. Files  : dmk.tpx
$
$ FILE DESCRIPTION
$ Netlist for the simulation circuit. Contains source, rectifier load,
$ active filter with switches and dc-sourc, and switched ripple filter
$
$ IMPORTANT NOTE
$ none
$
$ INPUT PARAMETERS
$ none
$
$ Developing System : IBM-PC
$ Tool              : Matlab, Version 5.2.0
$
$ Starting Date    : 02/20/2000
$ Update          : 07/25/2000
$
$-----

```

```

template circuit
<< vsa, vsb, vsc, vfdin
<% s1, s2, s3, s4, s5, s6, srf, addRL $, scrd
>> isa, isb, isc, vta, vtb, vtc, ira, irb, irc,
ird, vrd, il, ifa, ifb, ifc, vfa, vfb, vfc, ifd, vfd,
iva, ivb, ivc
{
$
$ source voltage input
v.vsa na1 gnd << vsa;
v.vsb nb1 gnd << vsb;
v.vsc nc1 gnd << vsc;
$
$ source voltage measurement
vm.vsam na1 gnd >> vsam;
vm.vsbm nb1 gnd >> vsbm;
vm.vscm nc1 gnd >> vsbm;
$
$ source current measurements
am.isa na1 na2 >> isa;

```

```

am.isb nb1 nb2 >> isb;
am.isc nc1 nc2 >> isc;
#
# source inductors
l.lsa na2 na3 = ?Ls;
l.lsb nb2 nb3 = ?Ls;
l.lsc nc2 nc3 = ?Ls;

r.rlsa na2 na3 = 1e5;
r.rlsb nb2 nb3 = 1e5;
r.rlsc nc2 nc3 = 1e5;
#
# source resistors
r.rsa na3 na4 = ?Rs;
r.rsb nb3 nb4 = ?Rs;
r.rsc nc3 nc4 = ?Rs;
#
# coupling point voltage measurements
vm.vta na4 gnd >> vta;
vm.vtb nb4 gnd >> vtb;
vm.vtc nc4 gnd >> vtc;
#
# cable inductors to nonlinear load
l.lca na4 na5 = ?Lc;
l.lcb nb4 nb5 = ?Lc;
l.lcc nc4 nc5 = ?Lc;
#
# cable resistance to nonlinear load
r.rca na5 na6 = ?Rc;
r.rcb nb5 nb6 = ?Rc;
r.rcc nc5 nc6 = ?Rc;
#
# nonlinear load current measurements
am.ira na6 na7 >> ira;
am.irb nb6 nb7 >> irb;
am.irc nc6 nc7 >> irc;
#
# rectifier diodes
d.d1 na7 nd1;
d.d3 nb7 nd1;
d.d5 nc7 nd1;
d.d4 nd2 na7;
d.d6 nd2 nb7;
d.d2 nd2 nc7;
#
# rectifier input path incl. smoothing components
am.ird nd1 nd3 >> ird;
l.lrd nd3 nd4 = ?Lrd;
r.rrd nd4 nd5 = ?Rrd;
c.crd nd5 nd2 = ?Crd, ?vcrd0;
#.s.crd nd2a nd2 <% (s.crd>=0.5), (s.crd<0.5);

vm.vrd nd5 nd2 >> vrd;
#
# dc load
am.il nd5 nd6 >> iL;
r.rL nd6 nd6a = ?RL;
r.rLadd nd6a nd7 = 80;
s.sLadd nd6a nd7 <% (addRL>=0.5), (addRL<0.5);
l.lL nd7 nd2 = ?LL;

```

```

#
# SRF capacitance
c.cva na4 na15 = ?Cv;
c.cvb nb4 nb15 = ?Cv;
c.cvc nc4 nc15 = ?Cv;
#
# SRF inductance
l.lva na15 na16 = ?Lv;
l.lvb nb15 nb16 = ?Lv;
l.lvc nc15 nc16 = ?Lv;
#
# SRF resistors
r.rva na16 na17 = ?Rv;
r.rvb nb16 nb17 = ?Rv;
r.rvc nc16 nc17 = ?Rv;
#
#
# SRF resistors
r.rva na4 na17 = ?Rv;
r.rvb nb4 nb17 = ?Rv;
r.rvc nc4 nc17 = ?Rv;
#
# SRF capacitance
c.cva na17 na19 = ?Cv;
c.cvb nb17 nb19 = ?Cv;
c.cvc nc17 nc19 = ?Cv;
#
# SRF currents
am.iva na17 na20 >> iva;
am.ivb nb17 nb20 >> ivb;
am.ivc nc17 nc20 >> ivc;
#
# on/off of SRF switches
s.srfa na20 gnd <% (srf>=0.5), (srf<0.5);
s.srfb nb20 gnd <% (srf>=0.5), (srf<0.5);
s.srfc nc20 gnd <% (srf>=0.5), (srf<0.5);
#
# active filter inductors
l.lfa na4 na10 = ?Lf;
l.lfb nb4 nb10 = ?Lf;
l.lfc nc4 nc10 = ?Lf;
#
# active filter resistors
r.rfa na10 na11 = ?Rf;
r.rfb nb10 nb11 = ?Rf;
r.rfc nc10 nc11 = ?Rf;
#
# active filter currents
am.ifa na12 na11 >> ifa;
am.ifb nb12 nb11 >> ifb;
am.ifc nc12 nc11 >> ifc;
#
# active filter output voltage
vm.vfa na12 gnd >> vfa;
vm.vfb nb12 gnd >> vfb;
vm.vfc nc12 gnd >> vfc;
#

```

```

%
% inverter switches
s.s1 na12 nf1 <% (s1>=0.5),(s1<0.5);
s.s3 nb12 nf1 <% (s3>=0.5),(s3<0.5);
s.s5 nc12 nf1 <% (s5>=0.5),(s5<0.5);
s.s4 nf2 na12 <% (s4>=0.5),(s4<0.5);
s.s6 nf2 nb12 <% (s6>=0.5),(s6<0.5);
s.s2 nf2 nc12 <% (s2>=0.5),(s2<0.5);
%
% dc path of active filter
am.ifd nf1 nf3 >> ifd;
v.vfd1 nf3 nf5 << vfdin;
v.vfd2 nf5 nf2 << vfdin;
vm.vfd nf3 nf2 >> vfd;
}

```

```

%RUN runs simulation in directory [OSU,MS]

```

```

%-----
%
% Author : Marcel Merk
% Date : 02/21/2000
%
% Add. Files : model.mdl
%
% FILE DESCRIPTION
% executes the SIMULINK simulation
%
% IMPORTANT NOTE
% none
%
% INPUT PARAMETERS
% none
%
% Developing System : IBM-PC
% Tool : Matlab, Version 5.2.0
%
% Starting Date : 02/21/2000
% Update : -
%
%-----

```

```

% init simulation -----
simfile = 'model'; % SIMULINK model

```

```

% runs simulation -----
eval(simfile); % open model
sim(simfile); % run simulation

```

```

% end of done -----

```

```

%PUBLISH plots waveforms of the project in the direcotry [OSU,MS]

```

```

%-----
%
% Author : Marcel Merk

```

```

% Date : 02/21/2000
%
% Add. Files : none
%
% FILE DESCRIPTION
% Plots the sampled waveforms of the last periode in the simulation.
%
% IMPORTANT NOTE
% none
%
% INPUT PARAMETERS
% workspace parameter created by init.m and simulink simulation
%
% Developing System : IBM-PC
% Tool : Matlab, Version 5.2.0
%
% Starting Date : 02/20/2000
% Update : -
%
%-----

```

```

% initialize -----
close all;
makeEPSfiles = 0; % produce eps prints
rootName = 'trans'; % root name of plots

```

```

% make calculations after simulation -----
calc;

```

```

% display options -----
Tshow = [0.1 0.1+(3/60)];
Fshow = [0 26];
xticks = 0.7+[0 0.5/60 1/60 1.5/60 2/60 2.5/60 3/60 ];
ShowGrids = 'on';

```

```

% plot waveforms -----
figure(20); % isout & icout (total)
yaxis = 40;
subplot(211);
plot(tAll,isout,'k');
hold on;
plot([tsrf_on tsrf_on],[-yaxis-5 yaxis+5],':k')
plot([taf_on taf_on],[-yaxis-5 yaxis+5],':k')
plot([tvl_on tvl_on],[-yaxis-5 yaxis+5],':k')
plot([tvl_off tvl_off],[-yaxis-5 yaxis+5],':k')
plot([thc_on thc_on],[-yaxis-5 yaxis+5],':k')
plot([tha_on tha_on],[-yaxis-5 yaxis+5],':k')
plot([tha_off tha_off],[-yaxis-5 yaxis+5],':k')
plot([0.9 0.9],[-yaxis-5 yaxis+5],':k')
hold off;
axisy([-yaxis yaxis]);
axisx([0 1]);
grid(ShowGrids);
norticks;
%placerticks(xticks);
%title('Source Current');
%xlabel('t [s]');
ylabel('i(t)_s_a [A]');

subplot(212);

```

```

plot(tAll,icout,'k');
hold on;
plot([tsrf_on tsrf_off],[-yaxis-5 yaxis+5],':k');
plot([taf_on taf_off],[-yaxis-5 yaxis+5],':k');
plot([tvl_on tvl_off],[-yaxis-5 yaxis+5],':k');
plot([thc_on thc_off],[-yaxis-5 yaxis+5],':k');
plot([tha_on tha_off],[-yaxis-5 yaxis+5],':k');
plot([0.9 0.9],[-yaxis-5 yaxis+5],':k');
hold off;
axisy([-yaxis yaxis]);
axisx([0 1]);
grid(ShowGrids);
%placerticks(xticks);
%title('Compensation Current');
xlabel('t [s]');
ylabel('i(t)_c_a [A]');

publish21S;

figure(21); % isout & icout (total)
subplot(311);
plot(tAll,irout,'k');
axisy([-25 25]);
axisx([0.9-2/60 0.9+4/60]);
grid(ShowGrids);
norticks;
placerticks([0.9-2/60 0.9-1/60 0.9 0.9+1/60 0.9+2/60 0.9+3/60 0.9+4/60]);
%title('Source Current');
%ylabel('t [s]');
ylabel('i(t)_r_a [A]');

subplot(312);
plot(tAll,isout,'k');
axisy([-25 25]);
axisx([0.9-2/60 0.9+4/60]);
grid(ShowGrids);
norticks;
placerticks([0.9-2/60 0.9-1/60 0.9 0.9+1/60 0.9+2/60 0.9+3/60 0.9+4/60]);
%title('Source Current');
%ylabel('t [s]');
ylabel('i(t)_s_a [A]');

subplot(313);
plot(tAll,icout,'k');
axisy([-25 25]);
axisx([0.9-2/60 0.9+4/60]);
grid(ShowGrids);
%norticks;
placerticks([0.9-2/60 0.9-1/60 0.9 0.9+1/60 0.9+2/60 0.9+3/60 0.9+4/60]);
%title('Source Current');
%ylabel('t [s]');
ylabel('i(t)_c_a [A]');

publish31S;

figure(22);
subplot(121);

```

```

stem([0:1023],abs(ir_f)*2,'k');
axisy([0 10]);
axisx([0 25]);
grid(ShowGrids);
%title('Load Current');
xlabel('Harmonic Number h [-]');
ylabel('|I(f)_r_a| [A]');

subplot(122);
stem([0:1023],abs(is_f)*2,'k');
axisy([0 10]);
axisx([0 25]);
grid(ShowGrids);
%title('Source Current');
xlabel('Harmonic Number h [-]');
ylabel('|I(f)_s_a| [A]');

publish12M;

% print results -----

fprintf(1,'\n\n');
fprintf(1,['h & Ir [A] & Ir [XX] & Is [A] & Is [XX] & ...'
' Ic [A] & Ic [XX] & Iv [A] & Iv [XX] & If [A] & If [XX]']);

fprintf(1,'\n 1 ');
fprintf(1,'%6.2f & %6.1f ',Ir_irms,Ir_irms/Ir_irms*100);
fprintf(1,'%6.2f & %6.1f ',Is_irms,Is_irms/Is_irms*100);
fprintf(1,'%6.2f & %6.1f ',Ic_irms,Ic_irms/Ic_irms*100);
fprintf(1,'%6.2f & %6.1f ',Iv_irms,Iv_irms/Iv_irms*100);
fprintf(1,'%6.2f & %6.1f ',If_irms,If_irms/If_irms*100);

fprintf(1,'\n 5 ');
fprintf(1,'%6.2f & %6.1f ',Ir_5rms,Ir_5rms/Ir_irms*100);
fprintf(1,'%6.2f & %6.1f ',Is_5rms,Is_5rms/Is_irms*100);
fprintf(1,'%6.2f & %6.1f ',Ic_5rms,Ic_5rms/Ic_irms*100);
fprintf(1,'%6.2f & %6.1f ',Iv_5rms,Iv_5rms/Iv_irms*100);
fprintf(1,'%6.2f & %6.1f ',If_5rms,If_5rms/If_irms*100);

fprintf(1,'\n 7 ');
fprintf(1,'%6.2f & %6.1f ',Ir_7rms,Ir_7rms/Ir_irms*100);
fprintf(1,'%6.2f & %6.1f ',Is_7rms,Is_7rms/Is_irms*100);
fprintf(1,'%6.2f & %6.1f ',Ic_7rms,Ic_7rms/Ic_irms*100);
fprintf(1,'%6.2f & %6.1f ',Iv_7rms,Iv_7rms/Iv_irms*100);
fprintf(1,'%6.2f & %6.1f ',If_7rms,If_7rms/If_irms*100);

fprintf(1,'\nn11 ');
fprintf(1,'%6.2f & %6.1f ',Ir_11rms,Ir_11rms/Ir_irms*100);
fprintf(1,'%6.2f & %6.1f ',Is_11rms,Is_11rms/Is_irms*100);
fprintf(1,'%6.2f & %6.1f ',Ic_11rms,Ic_11rms/Ic_irms*100);
fprintf(1,'%6.2f & %6.1f ',Iv_11rms,Iv_11rms/Iv_irms*100);
fprintf(1,'%6.2f & %6.1f ',If_11rms,If_11rms/If_irms*100);

fprintf(1,'\nn13 ');
fprintf(1,'%6.2f & %6.1f ',Ir_13rms,Ir_13rms/Ir_irms*100);
fprintf(1,'%6.2f & %6.1f ',Is_13rms,Is_13rms/Is_irms*100);
fprintf(1,'%6.2f & %6.1f ',Ic_13rms,Ic_13rms/Ic_irms*100);
fprintf(1,'%6.2f & %6.1f ',Iv_13rms,Iv_13rms/Iv_irms*100);
fprintf(1,'%6.2f & %6.1f ',If_13rms,If_13rms/If_irms*100);

```



```

fprintf(1,'\nTHD ');
fprintf(1,'%6.1f ',100*THD_Ir);
fprintf(1,'%6.1f ',100*THD_Is);
fprintf(1,'%6.1f ',100*THD_Ic);
fprintf(1,'%6.1f ',100*THD_Iv);
fprintf(1,'%6.1f ',100*THD_If);

fprintf(1,'\n\n');

fprintf(1,'\n\n Statistic of Load \n');
fprintf(1,'PL      = %6.2f W\n',PL);

```

```

fprintf(1,'Vrd      = %6.2f V\n',Vrd);
fprintf(1,'vrdrip = %6.2f %%\n',vrdrip*100);

```

```

fprintf(1,'\n\n');

```

```

% plot results -----
printepsfigs(rootName);

```

```

% end of publish.m -----

```

## E LIST OF MATERIALS FOR HARDWARE EVALUATION

Component	Part Number
DSP	TMS320F240
Evaluation board	TMS320C24X Evaluation Board
PAL	PALCE22V10
VT	LEM, LV24-P
CT	CR Magnetics Inc., CR8750-230
Opto coupler	6N136
Gate drive	IR2121
IGBT	IRG4PSH71KD
Snubber capacitor	IC, $1\mu F$